

EFFECTS OF WATER ON THE STRESS CORROSION CRACKING OF CARBON STEEL IN ETHANOLIC MEDIA


Fortunate Moyo

A research report submitted to the Faculty of Engineering and the Built Environment, University of the Witwatersrand, Johannesburg, in partial fulfilment of the requirements for the degree of Master of Science in Engineering

Johannesburg, 2013

DECLARATION

I declare that this research report is my own unaided work. It is being submitted to the degree of Master of Science in Engineering to the University of the Witwatersrand, Johannesburg. It has not been submitted before for any other degree or examination in any other University.

A handwritten signature in black ink, appearing to read 'F. Moyo', is written over a horizontal line.

Fortunate Moyo

5th day of February 2013

ABSTRACT

In this study, the effect of water on the stress corrosion cracking (SCC) of ASTM 516 in ethanol was investigated. Ethanol is hygroscopic in nature and its water content can increase rapidly when exposed to humid conditions. The presence of water in ethanol is likely to increase ethanol's oxygen content which is the major instigator of SCC.

In order to have an insight into the SCC susceptibility of carbon steel in ethanol-water solutions, the corrosion behaviour of the steel in these solutions was first evaluated. Carbon steel specimens in ethanol solutions with water exhibited various extents of localised corrosion, which increased in severity with increase in water content from 1 to 5 vol%. The occurrence of localised attack suggested that the presence of water promoted the formation of surface films; a condition suitable for SCC. Carbon steel specimens subjected to slow strain rate tests, however, exhibited ductile fractures indicating that the presence of up to 5vol% water did not induce SCC of carbon steel in ethanol.

To my parents

Kendu and Saziso Moyo

ACKNOWLEDGEMENTS

The support of the DST/NRF Centre of Excellence in Strong Materials (CoE-SM) towards this research is hereby acknowledged. I would also like to acknowledge the financial aid contributed by the University of Witwatersrand Postgraduate Merit Award.

I am grateful for the support of my supervisor, Josias Van Der Merwe, for his patience and insightful mentorship. My profound gratitude goes to the technical staff of the School of Chemical and Metallurgical Engineering especially Shadrack, Theo, Rhod, Phatu, Bruce and Doctor for their invaluable assistance. Great thanks to my fellow Masters students who made the year of my study enjoyable.

Lastly, but not least, I wish to thank and acknowledge the support of my family especially my sister Sanelisiwe.

CONTENTS

DECLARATION.....	i
ABSTRACT.....	ii
DEDICATION.....	iii
ACKNOWLEDGEMENTS.....	iv
CONTENTS	v
LIST OF FIGURES.....	ix
LIST OF TABLES.....	xi
LIST OF SYMBOLS.....	xii

CHAPTER ONE: INTRODUCTION.....	1
1.1 Motivation.....	1
1.2 Objectives.....	3
1.3 Hypothesis.....	3
1.4 Delimitations of the study.....	4
1.5 Technical Approach.....	4

CHAPTER TWO: LITERATURE REVIEW.....	5
2.1 Introduction.....	5
2.2 Ethanol.....	5
2.2.1 Production of ethanol.....	6
2.2.2 Chemical properties of ethanol.....	7
Ethanol and water.....	7
Ethanol and oxygen.....	8
2.3 Corrosion reactions.....	8
Charge transfer control.....	9
Diffusion control.....	10

Mixed control.....	10
2.4 Stress corrosion cracking.....	11
2.4.1 Definition of SCC.....	11
2.4.2 Mechanisms of SCC.....	13
Film rupture-Metal dissolution mechanism.....	13
Stress-sorption mechanism.....	14
Electrochemical mechanism.....	14
2.4.3 Crack morphology of SCC.....	15
2.4.4 SCC of carbon steel in ethanol environments.....	16
2.5 Monitoring corrosion processes.....	18
2.5.1 Linear polarisation resistance.....	19
2.5.2 Electrochemical impedance spectroscopy.....	20
The Nyquist plot.....	21
The Bode plots.....	22
CHAPTER THREE: EXPERIMENTAL METHODS.....	24
3.1 Introduction.....	24
3.2 Materials used.....	24
3.3 Electrochemical measurements.....	24
3.3.1 Apparatus.....	25
3.3.2 Sample preparation.....	26
3.3.3 Procedures.....	27
Linear polarisation resistance.....	27
Electrochemical impedance.....	27
3.3.4 Repeatability of the potentiostat.....	29
3.4 Slow strain rate test.....	30
3.4.1 Apparatus.....	30
3.4.2 Sample preparation.....	32
3.4.3 Procedures.....	33
Calibration of the stepper motor.....	33
SSRT.....	33
3.5 Solution characterisation.....	34

3.5.1 Apparatus.....	34
3.5.2 Procedures.....	34
Water content.....	34
Conductivity and dissolved oxygen.....	35
Acidity.....	35
3.6 Metallographic analysis.....	35
3.6.1 Apparatus.....	35
3.6.2 Procedures.....	36
3.7 Immersion test.....	36
3.7.1 Procedures.....	36

CHAPTER FOUR: RESULTS AND DISCUSSION

CORROSION CHARACTERISATION.....	38
4.1 Introduction.....	38
4.2 Solution characterisation.....	38
4.2.1 Conductivity.....	38
4.2.2 Dissolved oxygen.....	43
4.2.3 Acidity.....	46
4.3 Passivation tendencies.....	50
4.4 Corrosion mechanism.....	53
4.5 Corrosion rates.....	57

CHAPTER FIVE: RESULTS AND DISCUSSION

FAILURE ANALYSIS.....	61
5.1 Introduction.....	61
5.2 Characterisation of the carbon steel.....	61
5.3 SCC susceptibility.....	62
5.4 Surface examination.....	68

CHAPTER SIX: CONCLUSIONS.....	72
--------------------------------------	-----------

REFERENCES.....	74
------------------------	-----------

APPENDICES.....	80
------------------------	-----------

Appendix A: Water contents estimations.....	80
---	----

Appendix B: SSRT.....	83
-----------------------	----

LIST OF FIGURES

Figure 2.1: Flowchart showing the steps in the production of ethanol.....	6
Figure 2.2: The factors that contribute to SCC.....	11
Figure 2.3: A typical polarisation curve for an active/passive alloy.....	12
Figure 2.4: The effect of SCC on the load carrying thickness.....	13
Figure 2.5: SCC in brass exposed to ammonia.....	15
Figure 2.6 Schematic presentation of SCC cracking modes.....	16
Figure 2.7: SCC in steel equipment used in fuel ethanol.....	17
Figure 2.8: Crack velocity and water content in fuel ethanol.....	18
Figure 2.9: A linear polarisation plot.....	19
Figure 2.10: A typical Nyquist plot.....	22
Figure 2.11: Typical Bode plots.....	23
Figure 2.12: A typical equivalent circuit.....	23
Figure 3.1: Arrangement of the Autolab, water bath and Faraday cage.....	25
Figure 3.2: The corrosion cell inside the Faraday cage.....	26
Figure 3.3: Equivalent circuits used to evaluate EIS data.....	28
Figure 3.4: The tensile testing machine for SSRT without the corrosion cell.....	31
Figure 3.5: The corrosion cell used in the tensile test.....	32
Figure 3.6: Dimensions for SSRT specimens.....	32
Figure 3.7: The arrangement for measuring pHe.....	34
Figure 3.8: Dimensions for the immersion coupons.....	36
Figure 4.1: Conductivity of ethanol-water solutions before immersion.....	39
Figure 4.2: Solution resistance measured by EIS.....	41
Figure 4.3: Conductivity after 72 hours of immersion.....	42
Figure 4.4: Variation of dissolved oxygen with time and water content.....	44
Figure 4.5: Variation of pHe with water content.....	48
Figure 4.6: Change in water content after 90 days of immersion.....	49
Figure 4.7: Evolution of OCP with time for different ethanol-water solutions....	51
Figure 4.8: Double layer capacitance as a function of water content.....	52
Figure 4.9: Nyquist and Bode plots for the carbon steel specimens.....	54
Figure 4.10: Micrographs of the carbon steel after 72 hours of immersion.....	56

Figure 4.11: Variation in corrosion potential with water content.....	58
Figure 4.12: Corrosion rates estimated by LPR and weight loss.....	59
Figure 4.13: Variation of phase angle with water.....	60
Figure 5.1: Microstructure of the carbon steel.....	61
Figure 5.2: Percent elongation and area reduction as a function of water content.....	63
Figure 5.3: Variation of SCC ratios with water content.....	65
Figure 5.4: Stress-strain curves for the carbon steel specimens	66
Figure 5.5: Energy absorbed under different experimental conditions.....	68
Figure 5.6: Fractured specimens.....	69
Figure 5.7: Surface cracks of the carbon steel specimen.....	70
Figure 5.8: Fracture surface as viewed by SEM.....	71
Figure A.1: Calibration curve relating solubility and water content.....	81
Figure B.1: Calibration curve relating frequency and strain rate.....	84
Figure B.2: A typical stress-strain curve.....	85

LIST OF TABLES

Table 3.1: Composition of the carbon steel used.....	24
Table 3.2: Statistical analysis of repeatability test results.....	29
Table 4.1: Conductivity before immersion.....	39
Table 4.2: Ion product of water and ethanol.....	40
Table 4.3: Solution resistance as measured by EIS.....	41
Table 4.4: Conductivity after immersion.....	42
Table 4.5: Dissolved oxygen before immersion.....	44
Table 4.6: Dissolved oxygen after 72 hours of immersion.....	45
Table 4.7: Comparison of dissolved oxygen after and before immersion.....	45
Table 4.8: pHe measurements before immersion.....	47
Table 4.9: pHe measurements after 72 hours of immersion.....	47
Table 4.10: Estimated water content after 90 days of immersion	49
Table 4.11: Variation of OCP with time.....	50
Table 4.12: Double layer capacitance.....	52
Table 4.13: Corrosion potential of carbon steel in ethanol-water solution.....	57
Table 4.14: Corrosion rates by LPR.....	59
Table 4.15: Corrosion rates by weight loss.....	59
Table 5.1: Percent elongation and area reduction.....	62
Table 5.2: Predicting SCC susceptibility from SCC ratios.....	64
Table 5.3: UTS and energy absorbed before fracture.....	67
Table A.1: Statistical analysis of water content estimates.....	82
Table B.2: Calibration of the stepper motor.....	83

LIST OF SYMBOLS

A	Area [mm^2]
γ	Surface energy
pH	Negative logarithm of hydrogen ions in aqueous solutions
pHe	Negative logarithm of hydrogen ions in ethanol solutions
pKa	Negative logarithm of the acid dissociation constant
Ks	Ionic product
k	Conductivity [$\mu\text{S}/\text{cm}$]
I	Current [A]
E	Voltage [V]
ΔI	Change in current [A]
ΔE	Change in potential [V]
iR	Ohmic drop [V]
E_{corr}	Free corrosion potential [V]
I_{corr}	Corrosion current density [A/m^2]
β_a	Anodic Tafel constant [V/dec]
β_c	Cathodic Tafel constant [V/dec]
η	Overpotential [V]
η_A	Activation polarisation [V]
η_C	Concentration [V]
D	Diffusion coefficient [cm^2/s]
dC	Concentration gradient [mol/cm^3]
dx	The Nerst diffusion layer [cm]
R_p	Polarisation resistance [Ωm^2]
$R\Omega$	Ohmic resistance [Ω]

R_s	Solution resistance [Ω]
Cdl	Double layer capacitance [F/m^2]
f_{max}	Maximum frequency [Hz]
Z	Impedance [Ω]
Z''	Imaginary impedance [Ω]
Z'	Real Impedance [Ω]
ω	Angular frequency [Hz]
ϕ	Phase angle [$^\circ$]
σ	Tensile stress [MPa]
D_o	Original gauge diameter of tensile specimen [mm]
D_f	Final gauge diameter of tensile specimen [mm]
l_o	Original gauge length of tensile specimen [mm]
l_f	Final gauge length of tensile specimen [mm]
ϵ	Local dielectric constant [F/m]
ϵ^o	Permittivity of the air [F/m]
d	Film thickness [m]
S	Area of electrode [m^2]
Δt	Change in time
ρ	Density
m_b	Mass of coupon before exposure [g]
m_a	Mass of coupon after exposure [g]
n	Number of observations in the sample
x_i	The value of the i th observation
x_{mean}	Arithmetic mean
s	Standard deviation
s^2	Variance

Abbreviations

SCC	Stress corrosion cracking
SSRT	Slow strain rate test
UTS	Ultimate tensile strength
EIS	Electrochemical impedance spectroscopy
LPR	Linear polarisation resistance
SEM	Scanning electron microscope
IG-SCC	Intergranular stress corrosion cracking
TG-SCC	Transgranular stress corrosion cracking
OCP	Open circuit potential
Ag/AgCl	Silver-Silver chloride reference electrode
AC	Alternating current
FRA	Frequency response analyser
PSU	Power supply unit
DO	Dissolved oxygen
R1	Resistor 1
R2	Resistor 2
C2	Capacitor
W	Warburg resistor/ Warburg impedance
vol%	Volume percent
wt%	Weight percent

Chemical symbols

R-	Alkyl group
LiCl	Lithium Chloride
CH ₃ CH ₂ OH	Ethanol
CH ₃ COOH	Acetic acid

Acronyms

UN-Energy	United Nations Energy
ORNL	Oak Ridge National Laboratory
API	American Petroleum Institute
US	United States
ACE	Associated Chemical Enterprise
ASTM	American Society for Testing and Materials International
NACE	National Association of Corrosion Engineers International
ASM	American Society for Materials
NPL	National Physical Laboratory
REM	Renewable Energy Magazine

CHAPTER ONE

INTRODUCTION

1.1 Motivation

Most of the world's energy consumption originates from fossil sources such as coal, gas and oil. The concern surrounding the sustainability of these fuels has raised contentious debates and has increased the demand for alternative fuels. In addition to the depletion of their sources and their ever fluctuating prices, these fuels are associated with huge emissions of hydrocarbons and carbon dioxide, both of which are major contributors to global warming (Fergusson, 2001).

Biomass products such as bioethanol and biodiesel have been explored as potential alternative fuels to those that are petroleum-derived. Of these, bioethanol has gained significant interest because it can be used in all existing petrol engines without modifications. Popular ethanol blend fuel brands include E10 and E85 which contain 10 and 85% ethanol respectively. On the 23rd August 2012, South Africa's Department of Energy published regulations regarding mandatory blending of fuels with bioethanol (Herald, 2012); after announcing plans to invest R2 billion in an ethanol plant earlier in the year (Roelf, 2012). The move is in line with the world's trends towards 'greener' and less costly fuels.

The move to introduce this regulation is not only aimed at decreasing South Africa's carbon footprint but is also set to reduce her reliance on imported fuels. For a country reeling under very high unemployment rates, at 29.8% as of the first week of October 2011, (Statssa, 2012) the increase in ethanol production could also lead to increased job creation. RFA (2012) reported that in the USA, ethanol production was responsible for 90 200 direct jobs in 2011 alone. In addition, ethanol production could increase household income for the farming rural folk

and reduce the high rural-to-urban migration currently being experienced in the country (Statssa, 2012).

The world's leading consumers of bioethanol are Brazil, USA and Sweden, with 100% of Brazil's fuelling stations providing ethanol blended fuels (UN Energy, 2011). According to a report by ORNL (2008), these countries and others have reported occurrences of SCC of carbon steels exposed to ethanol fuels. Carbon steel is a very versatile form of steel. It has a wide range of engineering applications and its relatively low cost makes it an ideal material for projects requiring a lot of steel. In Brazil, carbon steels are commonly used in ethanol plants (Osterman, 2012) while in the USA, user terminals' storage tanks, pipes, loading/unloading racks are usually made of carbon steel (Beavers et al., 2008).

During their service lives, these structures are subjected to different forms of stress. Buried pipes, for example, may be subjected to subsidence of the ground while suspended pipes may experience stresses from misalignment during assembly or simply as a result of unevenly distributed dead loads. In addition, welding and machining of components often leaves them with high residual stresses, creating an ideal environment for SCC initiation (Scheel, 2010).

Extensive work has been done on the SCC of carbon steel in ammonia and carbonated solutions, yet little is understood on this phenomenon in ethanol. In the 1990s, the American Petroleum Institute (API) pioneered research into the SCC of carbon steel in ethanol and ethanol-blended fuels. Since then, there has been a growing interest in the phenomenon (Kane et al., 2004; Sridhar, 2006; Lou et al., 2009; Lou & Singh, 2011) with most work focused on the environmental factors that may affect SCC behaviour of carbon steel in ethanol and ethanol blended fuels. These studies recognised that the presence of certain impurities in ethanol affected its aggressiveness and therefore its ability to support SCC. One of these impurities is water.

Ethanol is hygroscopic in nature (Codd et al., 1972; Sridhar, 2006). If exposed to humid conditions, its water content will increase radically. During the production

of ethanol, water enters the ethanol stream as water vapour in the hot product. This, coupled with the fact that ethanol forms an azeotrope with water, it is almost impossible for an ethanol stream to have no water. Despite this, little analytical attention has been paid to the effect of water on the SCC behaviour of carbon steel in ethanol. Most studies have been based on high salt concentrations, yet in reality ethanol has very low salt impurities (Lou & Singh, 2011). It is therefore probable that at any given moment, a stream of ethanol would have a more significant concentration of water than salts.

In anticipation of high ethanol production, it is necessary to recommend ways to minimize SCC in carbon steels in contact with ethanol. The challenge is to understand the mechanism of degradation of carbon steel in ethanol-water mixtures so as to be able to predict the threshold water concentration for SCC and hence prevent this insidious form of corrosion.

1.2 Objectives

The objectives of this research are;

- 1) To study the corrosion characteristics of carbon steel in mixtures of ethanol and water.
- 2) To establish if ethanol-water mixtures can support SCC and hence determine the threshold water concentration, in the absence of aggressive salts, that can support SCC.
- 3) To ascertain if, in the absence of oxygen and ambient humidity, there is a change in the water content of ethanol in contact with carbon steel.

1.3 Hypothesis

The presence of water increases the quantity of oxygen in ethanol and influences the SCC susceptibility of carbon steel in ethanol solutions.

1.4 Delimitations of the study

This study was solely concerned with the effect of water on the SCC behaviour of carbon steel in ethanol solutions. Carrying out electrochemical tests in low conductivity medium is quite a challenge, which has led many authors to use supporting electrolytes such as sodium chlorides and perchlorates (De Souza, 1987; Lou, 2010; Bhola et al., 2011). However, for the present work, no supporting electrolyte was used. The effects of pressure, temperature, grain size and manufacturing history on the SCC of carbon steel were not considered.

1.5 Technical Approach

To achieve the goals mentioned in Section 1.2, solution characterisation, mechanical and electrochemical techniques were employed. The solution properties of the different ethanol-water mixtures as well as their potential as corrosives were characterized by evaluating their electrical conductivity and oxygen content. The acidity of the solutions was quantified by pHe.

Slow strain-rate tests (SSRT) were used to evaluate the susceptibility of carbon steel to SCC in various ethanol-water environments. Confirmation of the occurrence of SCC was done using a scanning electron microscope (SEM). Electrochemical impedance spectroscopy (EIS) and linear polarisation resistance (LPR) techniques were used to study the corrosion characteristics of carbon steel in ethanol-water solutions.

CHAPTER TWO

LITERATURE REVIEW

2.1 Introduction

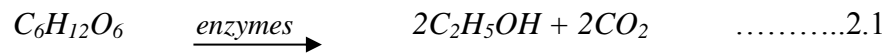
The interest in the phenomenon of stress corrosion cracking (SCC) in ethanol has been encouraged by the increased demand for ethanol caused by its growing application as a fuel and a fuel additive. To better understand this phenomenon, it is mandatory to study the basic concepts of SCC. An appreciation of ethanol, its production and its chemistry is necessary in order to understand and thus explain corrosion characteristics of carbon steel in this solvent. The aim of this section of the report is to address these matters, as well as to give an overview of the different types of corrosion reactions. A description of corrosion monitoring techniques is given.

2.2 Ethanol

Ethanol is a flammable liquid derived from carbohydrate raw materials. It is used in alcoholic beverages, antiseptics, cosmetics and perfume preparations, as well as in pharmacology. However, its largest single use is as a motor vehicle fuel and fuel additive. In 2011 alone, the world's production of ethanol for fuel consumption was estimated at 84 501 million litres (REM, 2012). Although ethanol fuel has been used in America since 1978, it only gained global interest recently, owing to governments becoming proactive in dealing with issues of global warming and the sustainability of petroleum derived fuels.

2.2.1 Production of ethanol

Ethanol is produced from a variety of organic sources including corn, barley, sugar cane, wheat, beverage waste and potato waste. The manufacture of ethanol is based on the microbiological action of yeast enzymes on sugars found in these sources. The fermentation reaction follows Equation 2.1 (Codd et al., 1972).



The agricultural feedstock is first hydrolysed before being subjected to the reaction in Equation 2.1. After fermentation, the product goes through rigorous dehydration stages to remove the water. The flowchart in Figure 2.1 gives the simplified steps for ethanol production using corn in the dry mill process.

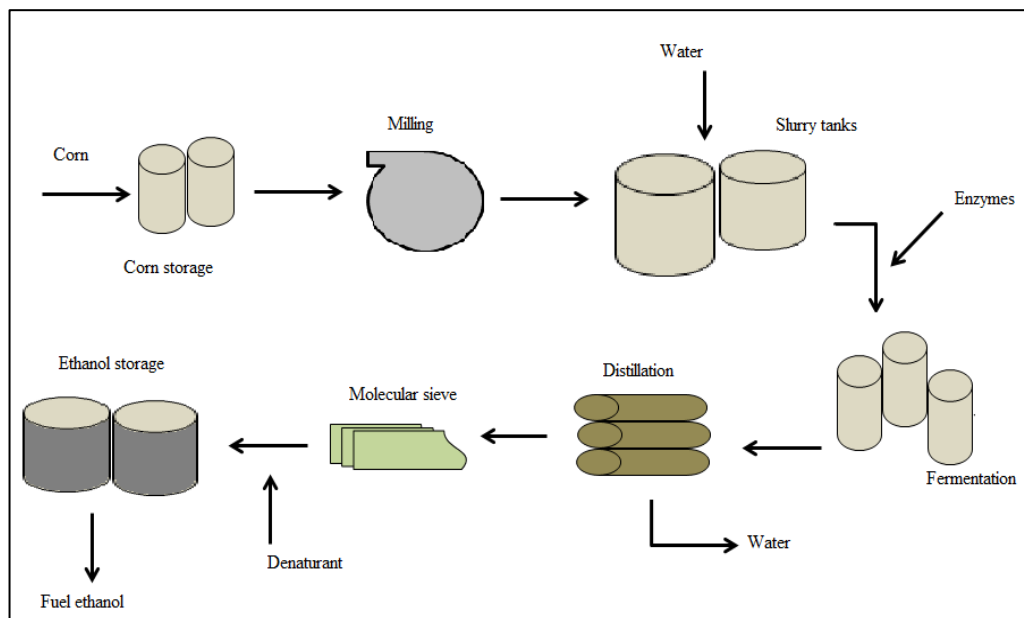


Figure 2.1: Flowchart showing the steps in the production of ethanol (derived from Naik et al., 2010).

The wide selection of feedstock means that any country in the world has the capacity to produce its own ethanol, and reduce dependence on imported fuels. This also means that any two streams of ethanol are likely to have different types and concentrations of contaminants such that their chemistry and hence potential as a corrosion medium would vary widely.

2.2.2 Chemical properties of ethanol

All alcohols, like water, are amphoteric. In the presence of water, alcohol will either be reversibly protonated or will dissociate slightly as given in Equations 2.2 and 2.3 (McMurry, 2007).



where R is the alkyl group $CH_3CH_2 -$ on ethanol. From these equations, it can be inferred that ethanol is a protic medium and just like water, is capable of sustaining electron transfer and ionization of hydrogen atoms (Kane et al., 2004). This thus implies that ethanol can support corrosion processes. The effects of water and oxygen on the chemical properties of ethanol are summarised below.

i. Ethanol and water

Ethanol is completely miscible in water since both solvents are polar in nature. The two liquids form an azeotropic mixture at 96% ethanol. During manufacture, ethanol and water are separated by azeotropic distillation techniques, namely molecular sieving as mentioned in Figure 2.1. Despite this, ethanol rarely has zero water. Ethanol is extremely hygroscopic in nature (Sridhar, 2006) and will absorb huge quantities of water when exposed to humid conditions.

The presence of water in ethanol has the effect of increasing the dielectric constant of ethanol (Faraji et al., 2009). Materials with a high dielectric constant break down easier when subjected to an electric field than those with a low dielectric constant. The consequence of this break down is an increased ability for the material to facilitate the flow of charge through it, and thus conduct electricity. Since increasing water content gives a corresponding increase in electrical conductivity, it means that increasing water increases the risk of corrosion in ethanol solutions.

The pKa of water is 15.74 while that of ethanol is 16 (McMurry, 2007). This implies that water is a stronger acid than ethanol. Its presence in ethanol should therefore increase the acidity of the solution.

ii. Ethanol and oxygen

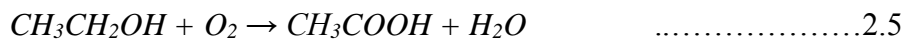
In fuels, the main benefit of ethanol is its ability to increase oxygen content and thus ensure complete combustion. Ethanol has a very high solubility for oxygen. At about 20°C, oxygen solubility in ethanol is 44 cm³/L compared to 6.4 cm³/L for distilled water at the same temperature (Reseder, 1980). Considering this difference, it should be expected that an increase in water content would markedly reduce oxygen solubility in ethanol.

Taking the solubility of oxygen to be a direct reflection of oxygen concentration in the solution, it follows therefore that the diffusion rates of oxygen in ethanol-water mixtures will be lower than in anhydrous ethanol. This inference can be supported by Fick's law of diffusion described in Equation 2.4 where D is the diffusion coefficient, dC is change in concentration and dx is the distance from electrode surface.

$$Flux = -D \frac{dC}{dx} \dots\dots\dots 2.4$$

According to this equation, if the concentration of a species in the bulk solution is high, then diffusion rates of that species will be high.

The oxidation of ethanol produces acetic acid as per Equation 2.5 (Tembe, 2010).

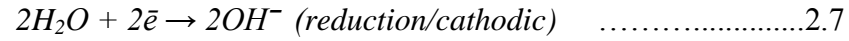
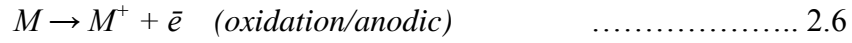


Organic acids are weak acids and are generally regarded as non-corrosive. Yet, they can hydrolyse well enough to act as true acids towards most metals (Scribner, 2001). The pKa of acetic acid at 25°C is 4.75 and its pH is 2.4. The oxidation of ethanol is thus associated with an increase in acidity and an increased corrosion risk.

2.3 Corrosion reactions

The theory of corrosion states that corrosion proceeds by an electrochemical reaction which can be divided into two or more oxidation and reduction reactions.

A metal, M, corroding in neutral water would thus react as per Equations 2.6 and 2.7.



When the metal, M, is not in equilibrium with its ions, for example when the anodic reaction is much faster than the cathodic reaction, the electrode potential, E , of M differs from its corrosion potential, E_{corr} , by an amount known as the overpotential or polarisation, η . This parameter is defined by Equations 2.8 and 2.9 (Roberge, 2008).

$$\eta = E - E_{corr} \quad \dots\dots\dots 2.8$$

$$\eta = \eta_A + \eta_C + iR \quad \dots\dots\dots 2.9$$

In Equation 2.9, η_A is the activation polarization, η_C is the concentration polarization and iR is the ohmic drop brought about by the electrical resistivity of the environment. In practice, one of the three potentials in the equation predominates (Codd et al., 1970; Simbi, 2006). This has led to the classification of three types of corrosion reactions.

i. Charge transfer controlled

A charge (or electron) transfer controlled reaction is characterised by a large activation potential, η_A . The activation potential of a corrosion reaction is a measure of how hard the anodic and the cathodic reactions must be driven to achieve the corrosion current and is strongly dependent on the composition of the solution.

Anions of low molar polarisation, when absorbed onto metal surfaces, have a poor tendency to promote electron exchange reactions and hence reduce the rate of electron transfer (Clubley, 1988; Simbi, 2006). Such anions substantially increase the activation potential and slow down corrosion processes. Inhibitors are examples of species that cause charge transfer controlled reactions.

Both water and ethanol have permanent dipoles arising from the asymmetric bonds between the oxygen and the hydrogen atoms. However, water molecules have a higher molar polarisation by virtue of their size. This implies that the presence of water in ethanol would improve the alcohol's tendency to promote electron transfer processes and increase corrosion rates.

ii. Diffusion-controlled

During a corrosion process, there exists a deviation of the concentration of the corroding species on the electrode surface from that in the bulk solution. This variation is described by Fick's law (Equation 2.4) and is characterised by the concentration polarization, η_c . A corrosion reaction whereby the slowest step involves a diffusion process is termed diffusion-controlled (Roseblim et al., 1968). The rate of such a reaction is increased by agitating the environment, increasing temperature and the concentration of the diffusing species.

Diffusion-controlled reactions are characterised by a limiting current density which is defined as the highest current density possible for a given electrode reaction due to the limitations imposed by the diffusion velocity of the reacting particles (Lapedes, 1978; Simbi, 2006). Corrosion processes of iron in water are controlled by the diffusion rate of oxygen to the corroding surface (Fontana, 1986; Revie, 2011) and the corrosion rate is usually determined by the limiting current density for the cathodic reduction of oxygen.

The corrosion processes in ethanol-water solutions are likely to be diffusion controlled given the low diffusion rates discussed in Section 2.2.2.

i. Mixed control

In mixed control processes, the rate of charge transfer is such that the concentration of one of the species decreases significantly at the interface (Pletcher, 1991) and differs greatly from its concentration in the bulk. This will give rise to a concentration gradient: the driving force for diffusion. As such, the

corrosion process is controlled by both the rate of charge transfer at the electrode and the diffusion of species to the electrode surface.

2.4 Stress corrosion cracking

2.4.1 Definition of SCC

Stress corrosion cracking is the spontaneous cracking of a metal resulting from the combined effects of stress and corrosion (Robertson, 1956). Figure 2.2 illustrates the interplay of these factors. The key damaging species in the corrosive environment need not be present in large concentrations (Yahalom & Aladjem, 1980; Simbi, 2006). In addition, the tensile stress may be applied stress, residual stress or a combination of both.

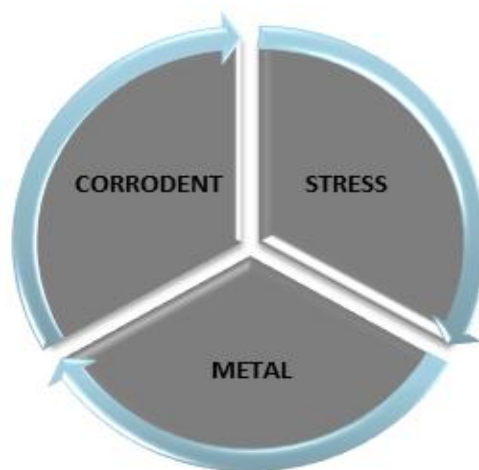


Figure 2.2: The factors that contribute to SCC (derived from Lou, 2010).

The SCC of an alloy in a particular environment is peculiar to that environment. It is imperative that the potential of the metal-corroduct system lies between the active and passive, or passive and transpassive regions (Yahalom & Aladjem, 1980; NPL 2000) (Figure 2.3).

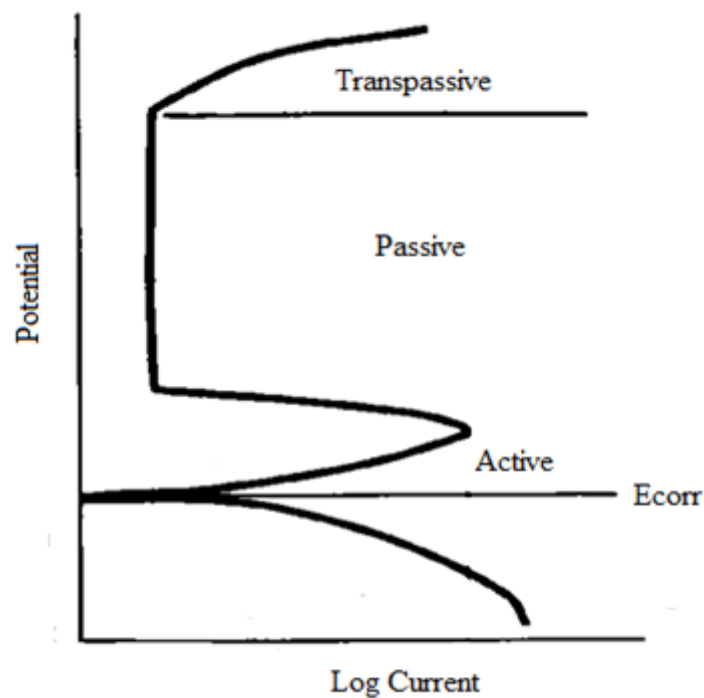


Figure 2.3: A typical polarisation curve for an active/passive alloy. (derived from Perry, 1999).

In service, the potential of a corroding system depends on the composition of the environment. The presence and concentration of cathodic reactants like water and oxygen (Fontana, 1986; NPL, 2000) in the environment can modify the potential of the system and profoundly influence the metal's susceptibility to SCC.

SCC is perhaps one of the most extreme forms of localised corrosion because it results in the sudden and unexpected failure of suitably matched engineering materials. This form of corrosion markedly reduces the load carrying capacity of the metal part (Rhodin, 1959; Yahalom & Aladjem, 1980), without significantly reducing its outer dimensions as illustrated in Figure 2.4.

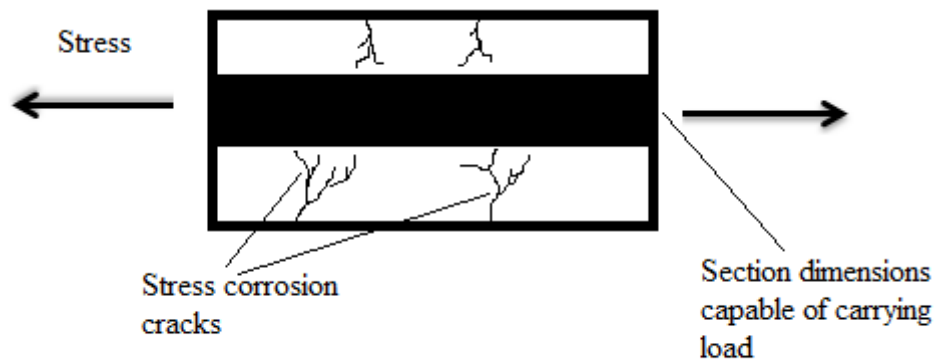


Figure 2.4: The effect of SCC on the load carrying thickness (derived from Yahalom & Aladjem, 1980).

2.4.2 Mechanisms of SCC

The occurrence of SCC can be explained by mechanisms that, in one way or another, involve anodic dissolution, the cleavage of the passive film or the absorption of some species into the metal's surface. Some of the proposed mechanisms for SCC are listed in this section.

i. Film rupture-Metal dissolution mechanism

This mechanism attributes SCC to the repeated rupture and repair of the protective film on the metal surface. The occurrence of SCC, especially in environments containing water, begins with the rupture of the relatively brittle passive film followed by metal dissolution, which results in the formation of a pit or a crevice where a crack eventually initiates and grows (ASM, 1987).

To promote SCC, it is crucial that there be a critical balance between the relative rates of metal dissolution and film repair. Environments that encourage active corrosion are most likely to result in high rates of metal dissolution and produce uniform or pitting corrosion rather than SCC, while passivating conditions will result in higher film repair rates, thus eliminating SCC (Arup & Parkins, 1975).

According to the film rupture-metal dissolution mechanism, it is necessary for the metal to passivate in the given environment. Passivity is not an inherent metal property (Uhlig, 1948), but depends entirely on the environment to which it is exposed. Many substances are capable of producing some degree of passivity, oxygen being the most common. However, for some metals like aluminium and titanium (Brown, 1977) water has been observed to perform this function just as well.

ii. Stress-sorption mechanism

In this mechanism, fractures result from the production of a brittle region at the crack tip because of the absorption of specific species into the metal (Yahalom & Aladjem, 1980). An example is hydrogen embrittlement. In acidic media, hydrogen production may result from the cathodic reaction as shown in Equation 2.8.



In neutral media, hydrogen ions may be produced by a chemical reaction between the exposed metal and water within confined volumes such as crack tips and crevices (Equation 2.9). The ions thus produced are subsequently reduced as per Equation 2.8 to give hydrogen gas.



Hydrogen atoms, because of their small size, have a high diffusivity in the metal lattice. The absorbed hydrogen atoms interact with strain bands in the crack tip and reduce the surface energy, γ , in this region. This compromises the mechanical properties of the metal by lowering the stress required to produce a brittle fracture.

iii. Electrochemical mechanism

The electrochemical theory of SCC proposes that in the alloy, there must exist the susceptibility to selective corrosion along a more or less continuous path (Uhlig, 1948). Microstructural differences give rise to electrochemically distinct

regions (Arup & Parkins, 1975), especially where there is the segregation of one species to the grain boundaries. Grain boundaries are usually anodic to the material within the grains (ASM, 1987) and will therefore be preferentially dissolved when exposed to the corrosive medium. This results in intergranular corrosion and the extent of grain boundary penetration plays a significant role in SCC susceptibility in the given media. The crack path coincides with the corrosion path.

In low carbon steels, carbon tends to segregate to the ferrite grain boundaries as carbon or carbide precipitates (Arup & Parkins, 1975). The carbon enriched boundaries then become anodic to the adjacent grains, and the small anode to cathode ratio that results becomes the driving force for intergranular corrosion. Under the simultaneous influence of stress, the steel would fail by intergranular SCC (IG-SCC).

2.4.3 Crack morphology of SCC

Stress corrosion cracking normally appears as a multi-branched brittle fracture perpendicular to the direction of the stress. These characteristics are illustrated in Figure 2.5 which shows stress corrosion cracks in brass as a result of exposure to ammonia.



Figure 2.5: SCC in brass exposed to ammonia (display specimen, courtesy of Metallography Lab, Metallurgical Engineering, University of the Witwatersrand)

Figure 2.5 shows secondary cracks branching off from the larger primary crack. The corrosion products accumulate along the cracks and outline the morphology of the secondary cracks. Considering Figures 2.4 and 2.5, the final fracture would then consist of two distinct zones: a zone formed by the propagation of corrosion cracking, with traces of corrosion products, and a zone produced by the mechanical failure of the metal.

SCC can either be transgranular (TG-SCC) or intergranular (IG-SCC). In TG-SCC, crack propagation is through the grains while in IG-SCC, it is along the grain boundaries as illustrated in Figure 2.6.

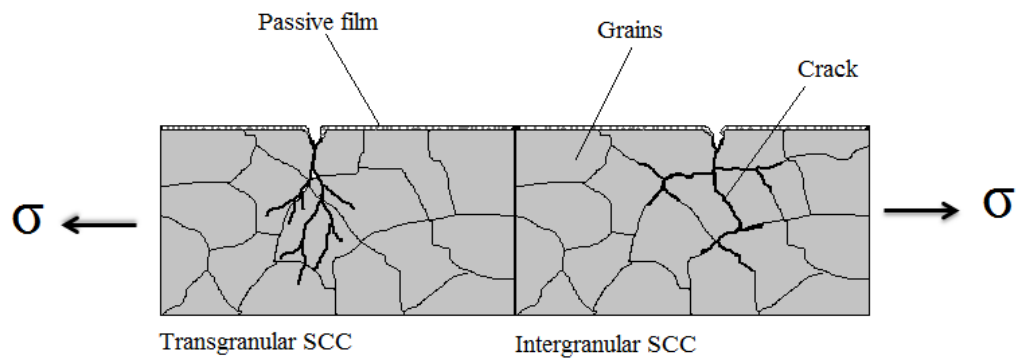


Figure 2.6: A schematic presentation of SCC cracking modes (derived from HILTI, 2000).

While TG-SCC is not uncommon in carbon steels, the metal is more prone to fail by IG-SCC (Arup & Parkins, 1975). This suggests that SCC in carbon steels is associated with intergranular corrosion.

2.4.4 SCC of carbon steel in ethanol environments

Carbon steels can suffer from SCC in environments that tend to form passivating films (NPL, 2000). While the science of SCC of carbon steel in ethanol and ethanol blended fuels is not well understood, the fact that it occurs implies that carbon steel has some tendency to passivate in these solutions. Figure 2.7 shows SCC of carbon steel reproduced in a lab using fuel ethanol (Lou, 2010).

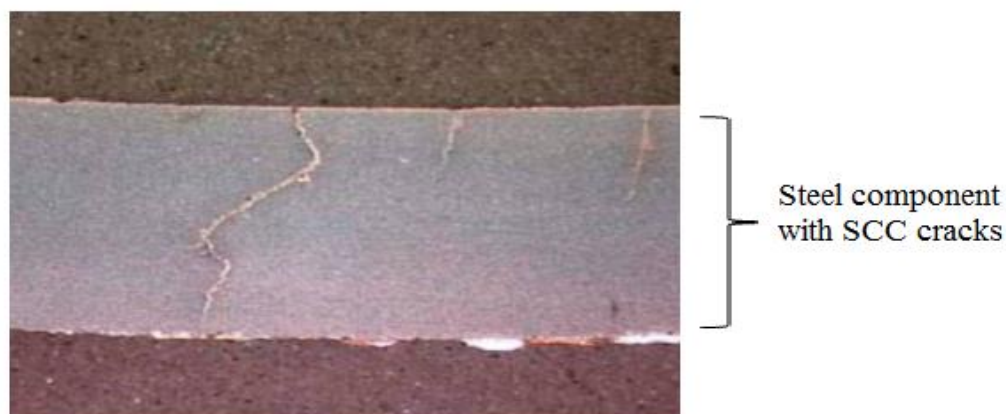


Figure 2.7: SCC in carbon steel used in fuel ethanol (Lou, 2010).

Several researchers have found oxygen to be the key factor in ethanol related SCC (Kane et al., 2004; Beavers et al., 2008; Lou et al., 2009). Specimens exposed to deaerated ethanol solutions exhibited high ductility and no cracking, even in the presence of aggressive species like chloride. The need for oxygen would suggest that SCC of carbon steel is by the film rupture-metal dissolution mechanism. However, in 2008, Newman proposed that ethanol is oxidised in cracks to form acetic acid and possibly lead to intergranular corrosion and subsequently IG-SCC. In both cases, the presence of oxygen, or at least an oxidising agent, is essential for SCC to occur in ethanol.

The role of water in the corrosion of metals in non-aqueous environments has been widely studied (de Anna, 1985; Brossia, 1995; Bhola et al., 2011), with much focus being on methanol. Brossia, (1995) showed that the presence of water in acidic methanol caused passivity and significantly hindered corrosion. Goodman and Singh (2010) observed a similar behaviour with ethanol where 1 vol% water caused rapid passivation of carbon steel. The findings indicate that water can act as an oxidiser, capable of promoting passivation processes on metal surfaces.

Water contents ranging from 170 ppm to 1 wt% do not have a significant effect on SCC of carbon steel in ethanol (Sridhar, 2006). Lou et al. (2009) showed that at 1 vol% water, crack velocity was at its highest at almost 4.5×10^{-7} mm/s (Figure 2.8). This implies that at 1vol% water, carbon steel is most susceptible to

SCC. The apparent contradiction between these studies can be explained by considering that 1 vol% is larger than 1 wt% water. However, the presence of the aggressive chloride ions in the solutions used in these two studies may have affected the passivity of the metal, and influenced susceptibility to SCC.

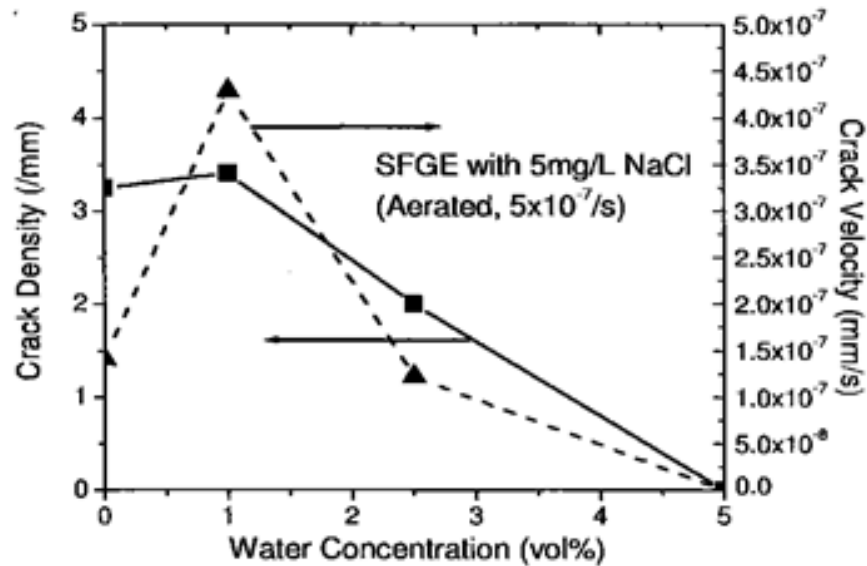


Figure 2.8: Relationship between crack velocity and water content in fuel ethanol (Lou, 2010).

In contents greater than 1 vol%, water can slow down the repassivation kinetics of carbon steel in ethanol (Lou & Singh, 2011). According to Arup and Parkins (1975), if passivation is too slow, pitting is more likely than cracking because of sustained anodic activity. As such, susceptibility to SCC should be expected to decrease with an increase in water content. Two other independent studies (Lou et al., 2009; Goodman & Singh, 2010) arrived at a similar conclusion that at higher water contents, passivation behaviour changed the mode of failure from SCC to pitting.

2.5 Monitoring corrosion processes

Detecting corrosion and measuring corrosion rates can be done by the use of electrochemical techniques. While every technique may have its advantages, it is

essential to complement it with other measuring techniques. By so doing, a more accurate picture of the electrode processes may be obtained.

2.5.1 Linear polarisation resistance

Linear polarisation resistance (LPR) measuring techniques involve an iR drop through the electrolyte surrounding the electrode and/or through a surface film. It is a useful method for determining instantaneous corrosion rates and is both rapid and non-intrusive (Song & Saraswathy, 2000). In addition, LPR can give the corrosion potential of a metal in contact with an electrolyte which is in fact, an indication of the tendency of a metal to corrode in that environment.

Under potentiostatic conditions, LPR is conducted by changing potential at a constant rate, ΔE and monitoring the change in current, ΔI . The rate of corrosion is determined from linear polarisation plots which relate ΔE and ΔI . A linear polarisation resistance plot is given in Figure 2.9.

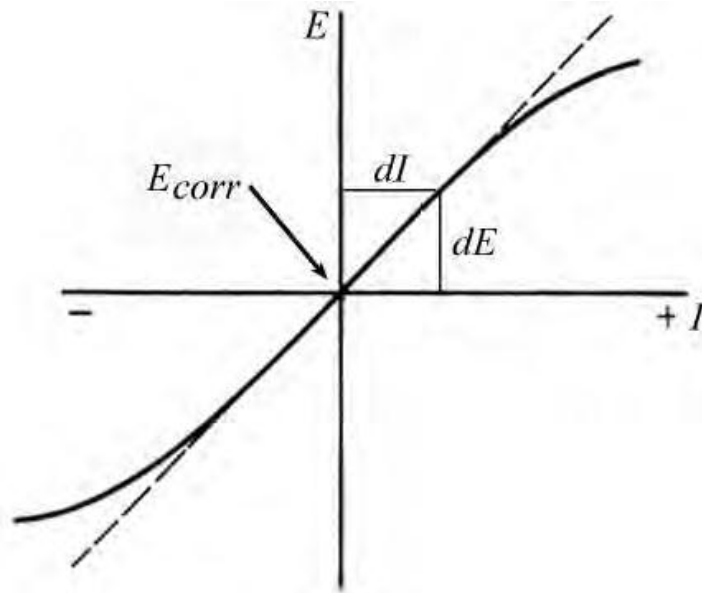


Figure 2.9: A linear polarisation resistance plot (Nygaard, 2008).

The corrosion rate is expressed by the Stern-Geary equation

$$i_{corr} = \left[\frac{\beta_a \beta_c}{2.303(\beta_a + \beta_c)} \right] \left(\frac{1}{R_p} \right) \dots\dots\dots 2.10$$

In Equation 2.10, i_{corr} is the corrosion current density, R_p is the polarisation resistance and β_a and β_c are the anodic and cathodic Tafel constants respectively. The value of R_p is the gradient of the linear polarisation plot (Figure 2.9) within 10-30 mV more noble or more active than E_{corr} , the free corrosion potential.

The main limit of LPR is that it is often erroneous when used in environments in which the electrolyte has significantly high resistivity. In such cases it should be complimented by other electrochemical techniques such as EIS.

2.5.2 Electrochemical impedance spectroscopy

Electrochemical Impedance Spectroscopy (EIS), also referred to as AC impedance analysis, is a technique used to investigate the corrosion behaviour of metals in low conductivity solutions. It is a non-destructive technique in which a small sinusoidal voltage is superimposed on an applied potential at predetermined discrete frequencies. The current responses to these perturbations are used to determine impedance (resistance), Z , as defined by Equation 2.11 (Pletcher, 1991).

$$E = IZ \dots\dots\dots 2.11$$

E is the applied voltage and I is the current. The analysis of EIS data involves the use of passive elements like resistors, capacitors and inductors and these elements represent some physical component of the corroding system. Listed below are some of the common passive elements and their interpretation.

- i. **R_Ω** : Referred to as the ohmic resistance, R_Ω is the resistance between the working electrode and the reference electrode. It is used to characterise the resistance of the solution and its value is determined at the high frequency end of the impedance spectrum.
- ii. **R_{ct}** : R_{ct} is the charge transfer resistance which characterises the electron transfer process in corrosion.

- iii. **R_p**: R_p is the polarisation resistance that arises from the polarisation of the working electrode. Polarisation resistance is related to the corrosion rate by the Stern-Geary relationship given in Equation 2.10.
- iv. **C_{dl}**: This refers to the double layer capacitance and is related to the double layer formed as the ions in the solution approach the electrode surface (Metrohm, 2011). The double layer capacitance is closely related to the thickness, *d*, of the film formed on the surface by Equation 2.12 (Ebrahim et al., 2012).

$$C_{dl} = \frac{\epsilon^o \epsilon}{d} S \quad \dots\dots\dots 2.12$$

In this equation, ϵ^o and ϵ are the permittivity of air and the local dielectric respectively and *S* is the surface area of the electrode.

- v. **W**: Known as the Warburg impedance or the diffusion impedance, this quantity models the diffusion of ionic species at the interface (Metrohm, 2011) and can be used to qualify diffusion controlled corrosion processes.

Experimental data from EIS is presented in a wide range of plots, but only two will be discussed here.

i. The Nyquist plot

This is a plot of the imaginary component of impedance, *Z''* against the real part of impedance, *Z'*. A typical Nyquist plot is shown in Figure 2.10.

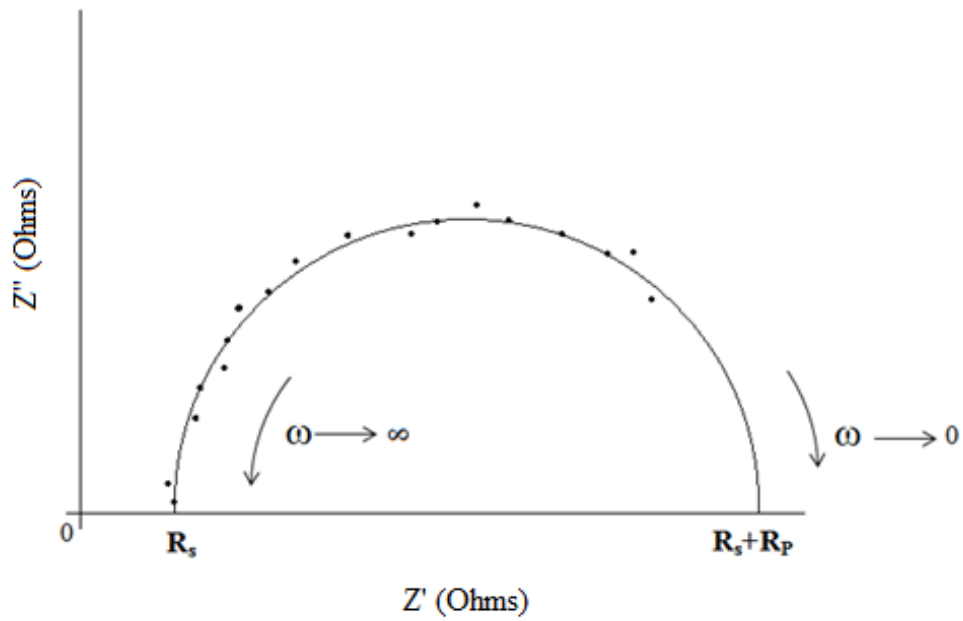


Figure 2.10: A typical Nyquist plot (derived from MacDonald, 1992).

The intersection of the plot with the x -axis at the high frequency end ($\omega \rightarrow \infty$) gives the solution resistance, while the intersection at the low frequency end ($\omega \rightarrow 0$) gives the sum of the polarisation resistance and solution resistance.

ii. The Bode plots

There are two types of Bode plots. One gives the relationship between the logarithm of the modulus of impedance, $\log |Z|$ and the logarithm of angular frequency, $\log \omega$. The second is the relationship is between the phase angle, ϕ (which is the angle between the potential perturbation and the response current) and the logarithm of angular frequency $\log \omega$. Figure 2.11 gives a typical Bode plot.

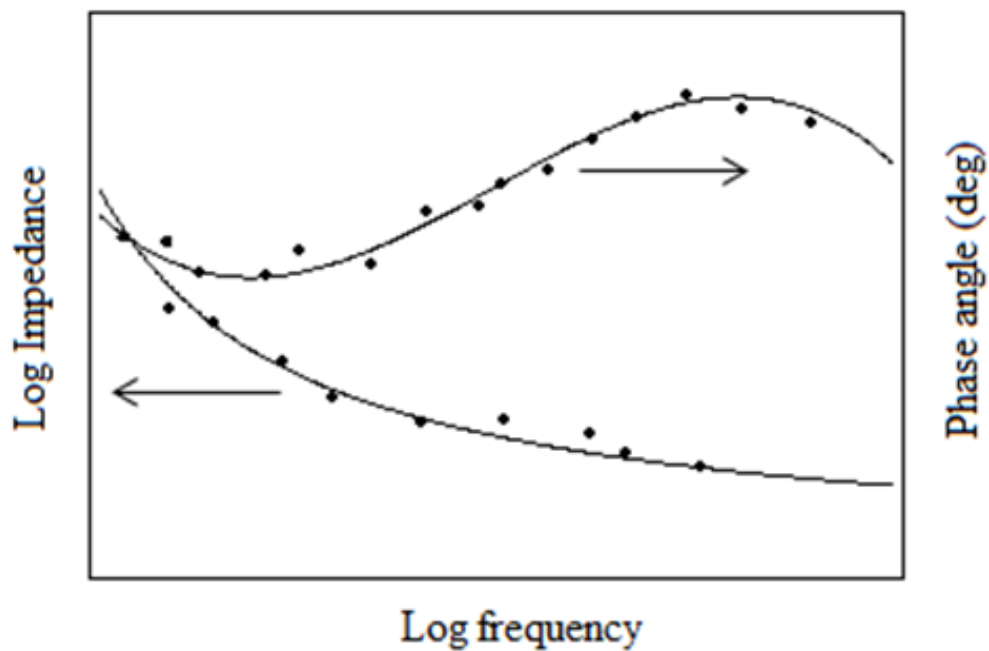


Figure 2.11: Typical Bode plots (derived from Blue & Moran, 1990).

For a comprehensive analysis of impedance data, the Nyquist and Bode plots must be used together. The dots shown in Figures 2.10 and 2.11 represent the actual data obtained during experimentation, while the solid lines is obtained when the data is fitted onto an equivalent circuit. An equivalent circuit is made by combining the passive element discussed earlier, either in series or in parallel, and is used to model the different processes occurring at the corrosion interface. Figure 2.12 gives one such equivalent circuit. The values of the various elements of the circuit can be used to quantify corrosion processes.

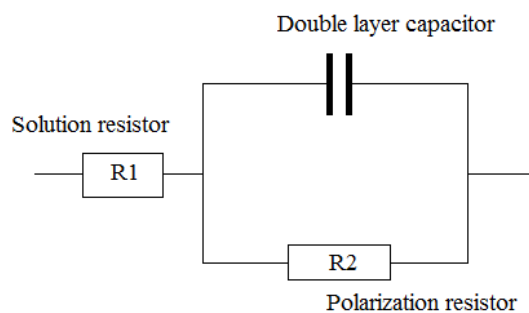


Figure 2.12: A typical equivalent circuit (derived from Metrohm, 2011).

CHAPTER THREE

EXPERIMENTAL METHODS

3.1 Introduction

This chapter gives a detailed description of the apparatus and experimental procedures used to achieve the objective of the study.

3.2 Materials used

The alcohol used in these experiments was analytical grade obtained from Associated Chemical Enterprises (ACE), South Africa. It contained approximately 0.02% water, 0.0001% iron, 0.003% acetic acid and at least 99.8% ethanol. The chemical was used in the as-received condition without further purification.

The carbon steel used was ASTM 516 Gr 60 obtained from VRN Macsteel in the form of 12 mm plate. A spark analysis revealed that the steel contained the elements shown in Table 3.1.

Table 3.1: Composition of the carbon steel used (wt%).

Carbon	Manganese	Silicon	Sulphur	Phosphorus
0.17	0.95	0.24	≤0.005	0.019
Chromium	Nickel	Copper	Aluminium	Iron
0.03	≤0.01	≤0.01	0.028	Balance

3.3 Electrochemical measurements

The electrochemical techniques used to monitor the corrosion of carbon steel in hydrated ethanol were electrochemical impedance spectroscopy (EIS) and linear polarisation resistance (LPR). The measurements were achieved potentiostatically as per ASTM G3-89. Potentiostatic techniques function by maintaining potential

constant and measuring the current response. These methods were preferred to galvanostatic techniques because the resulting data are easier to interpret and are particularly useful when determining the effect of environmental changes on reaction rates (Greene, 1965).

3.3.1 Apparatus

All electrochemical measurements were carried out with a Metrohm PGSTAT302 Autolab potentiostat shown in Figure 3.1. The corrosion cell was placed in a grounded Faraday cage shown on the left in the figure.



Figure 3.1: Arrangement of the Autolab, water bath and Faraday cage for electrochemical measurements.

The electrochemical measurements were carried out in a 3-electrode corrosion cell (Figure 3.2). A Ag/AgCl, LiCl in Ethanol reference electrode was used with a graphite counter electrode. The reference electrode was placed in a Luggin capillary and to minimise the effect of iR drop, the capillary tube was placed at about 3 mm from the working electrode (Roberge, 2008). Care was taken to fill the Luggin capillary with the test solution so as to ensure that the reference

electrode was immersed in the electrolyte at all times. Both the Luggin capillary and the corrosion cell were cleaned with detergent and distilled water before use.

The arrangement of the corrosion cell in the Faraday cage is shown in Figure 3.2. Tubes were used to circulate water to the corrosion cell to maintain the temperature of the environment at $25 \pm 1^\circ\text{C}$. The software used to capture the electrochemical measurements was NOVA 1.7 from Metrohm.

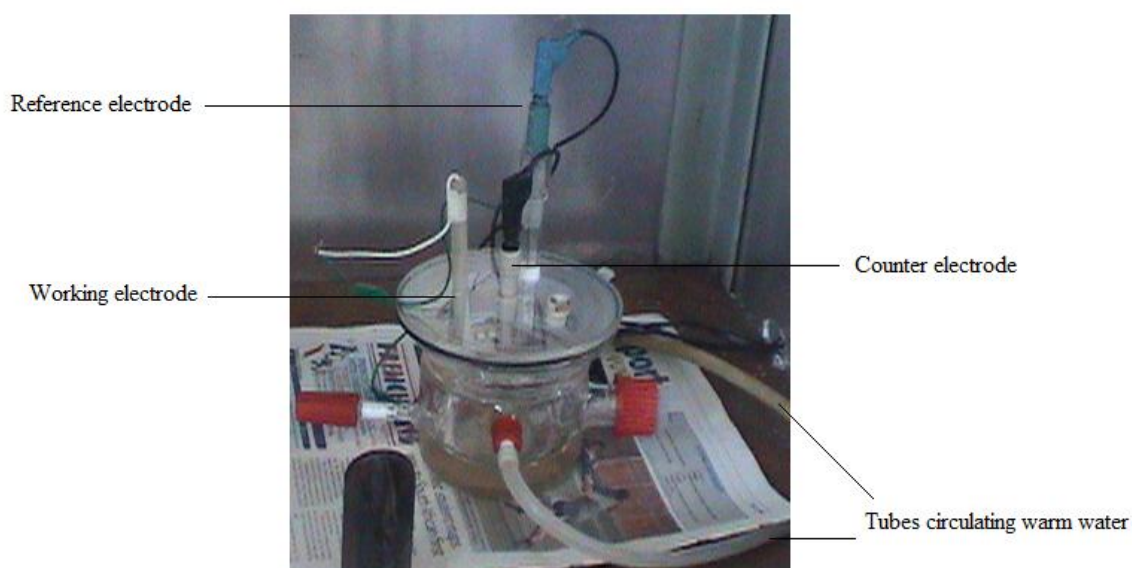


Figure 3.2: The electrochemical corrosion cell inside the Faraday cage.

3.3.2 Sample preparation

When performing EIS measurements in liquid dielectrics, it is important to use a small working electrode (MacDonald, 1992). Thus, the corrosion samples used in this study were cut to about 0.25 cm^2 . They were connected to a copper wire by means of a conducting aluminium tape, mounted in an epoxy resin and cured at room temperature for at least 12 hours.

Before immersion, the mounted samples were progressively abraded using a series of emery papers of decreasing grit size, ranging from 240 to 1200. The samples were cleaned and degreased in ethanol. The time between the final

surface preparation and the start of the experiment was kept to no more than 2 hours. This was done so as to improve repeatability.

3.3.3 Procedures

i. Linear polarisation resistance

The test environments were made by placing known volumes of water into a 500 ml beaker and filling up with ethanol to the 500 ml mark. No supporting electrolytes or salts were added to the solution. The linear polarisation measurements were carried out at a scan rate of 0.5 mV/s. Open circuit potential (OCP) values were recorded at a 12 hour interval over a period of 72 hours.

ii. Electrochemical impedance

The solutions used were prepared as in the procedure for linear polarisation resistance. Measurements were done at frequencies ranging from 80 Hz to 0.01 Hz at amplitudes of 10 mV. The low frequency limits were chosen to ensure minimal changes in the system, and therefore guarantee linearity conditions. A frequency response analyser, FRA, was used in conjunction with NOVA 1.7 to collect impedance data.

The equivalent circuits used to evaluate EIS data are given in Figure 3.3.

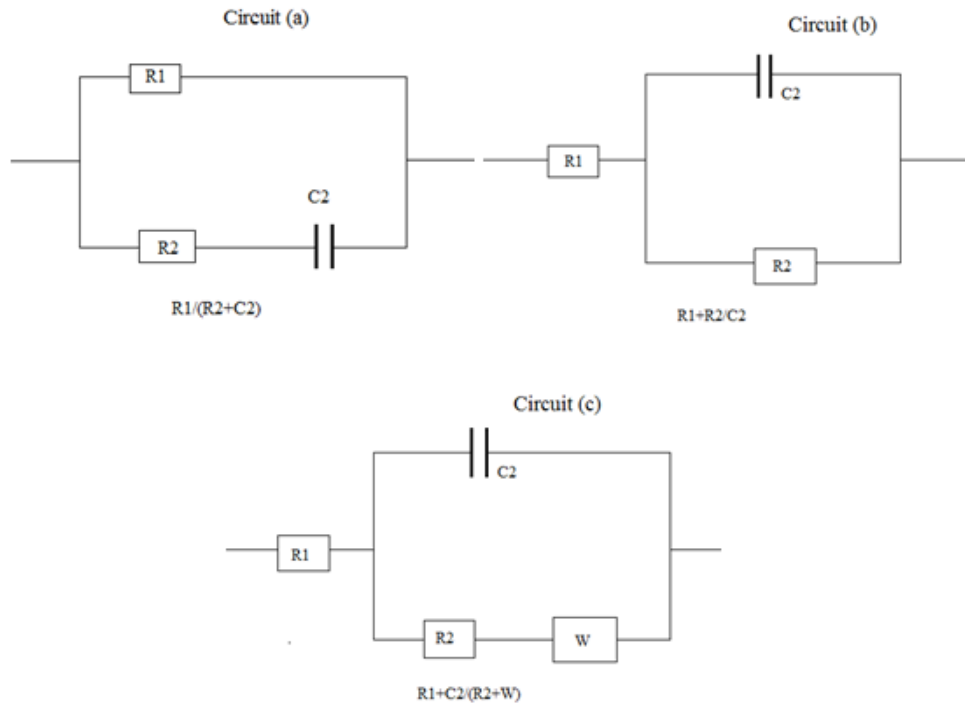


Figure 3.3: Equivalent circuits used to evaluate EIS data

Circuits (a) and (b) were used to analyse the data obtained from experimentation in ethanol solutions containing no water and with 1 vol% water. These circuits are non-distinguishable (Bio-Logic, 2011) and are therefore interchangeable. In circuit (b), R_1 is equivalent to R_Ω , the solution resistance while R_2 is equal to the polarisation resistance, R_p . In circuit (a), R_1 is equivalent to R_p while the solution resistance is expressed by Equation 3.1 (Bio-Logic, 2011)

$$R_\Omega = \frac{R_1 \times R_2}{R_1 + R_2} \dots\dots\dots 3.1$$

For the analysis of carbon steel specimens in ethanol with 2.5 and 5 vol% water, Circuit (c) was used. The choice of the circuits was based on the shapes of the Nyquist curves obtained in the preliminary stages of the study. The curves for the specimens in the solutions with 2.5 and 5 vol% water were characterised by a Warburg slope thus necessitating the integration of the Warburg impedance into Circuit (c).

The double layer capacitance was calculated using Equation 3.2.

$$C_{dl} = \frac{1}{2\pi f_{max} R_p} \dots\dots\dots 3.2$$

3.3.4 Repeatability of the potentiostat

The precision of a measuring technique lies in its ability to reproduce its own results (Shoukri, 2004). The repeatability of the potentiostatic measuring method was determined by carrying out two OCP tests in anhydrous ethanol. Presented in Table 3.2 are the results of the statistical analysis of the obtained results.

Table 3.2: Statistical analysis of repeatability test results

Time (h)	First test (mV)	Second test (mV)	Average OCP (mV)	Difference
0	217	201	209.0	-16
12	281	282	281.5	1
24	282	293	287.5	11
36	289	308	298.5	19
48	271	290	280.5	19
60	300	311	305.5	11
72	305	314	309.5	9
			Mean Difference	7.7
			Standard deviation of difference	12.1

The standard deviation of the differences is 12.1 and the coefficient of repeatability, r , is twice this value (24.2mV).

Mean difference is the mean of the differences of the results of the two tests. In this case, the mean is 7.7. Since the same method was used, under identical conditions and by the same researcher, the mean difference should ideally be zero. However, the mean difference in this analysis is not significantly further from

zero. Given this, the repeatability and hence precision of the measuring technique is fairly good.

3.4 Slow strain-rate test

The criterion given in the NACE standard TM0111-2011 was used to characterise SCC susceptibility of carbon steel in various ethanol-water solutions. The possibility that specimen failure under tensile loading may be as a consequence of simple void coalescence and not SCC was considered, and metallographic examination, by use of optical and scanning electron microscopes (SEM), was done to confirm the occurrence of SCC.

3.4.1 Apparatus

The slow strain-rate tensile testing machine used is shown in Figure 3.4. It is a screw-driven type of machine. Button-head (shouldered) grips were used to hold the specimens. These were designed in such a way that the grips would self-align along the vertical axis upon application of loads, thus minimizing chances of eccentrically loading the specimens.

The speed at which the screw rotated, and hence the speed of the crosshead, was controlled by means of a 23HSX-101 stepper motor. The software used to monitor changes in load with time was Smart PDC 2010.

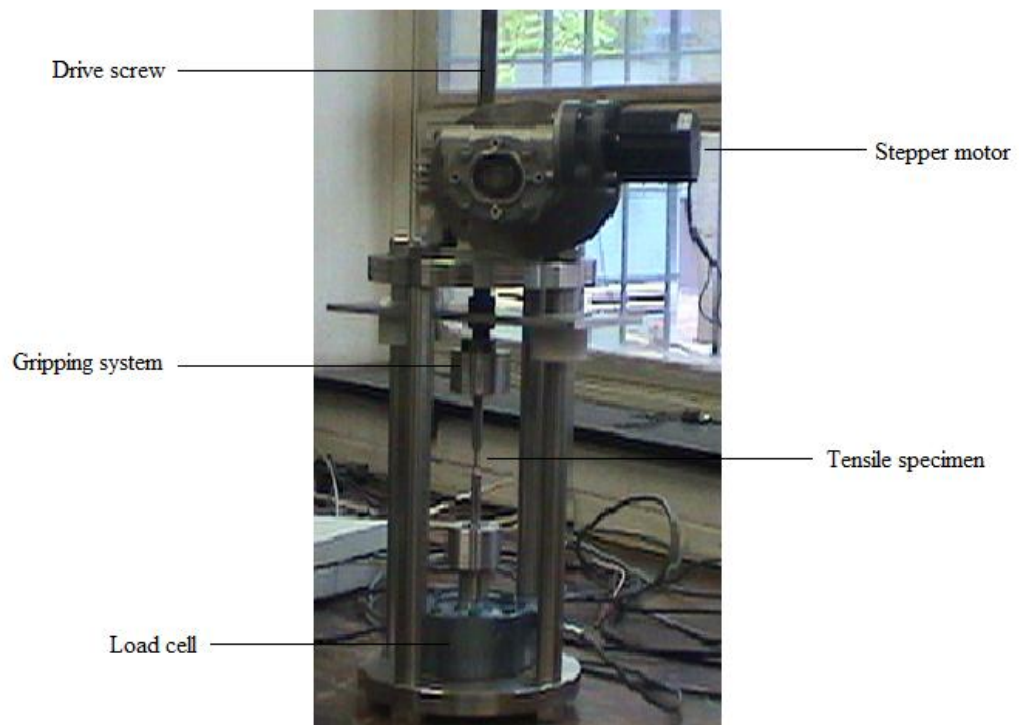


Figure 3.4: The tensile testing machine for SSRT without the corrosion cell.

A signal generator, together with a driving circuit consisting of a Gecko G230V stepper drive, an 8A PSU board and a 32VAC transformer, was used to drive the motor. The stepper motor-signal generator combination was calibrated to determine the variation of strain-rate with the frequency of the generated pulse.

The corrosion cell used in this procedure, shown in Figure 3.5, was designed from stainless steel. A heat controller was used to maintain the temperature at $25 \pm 1^\circ\text{C}$.

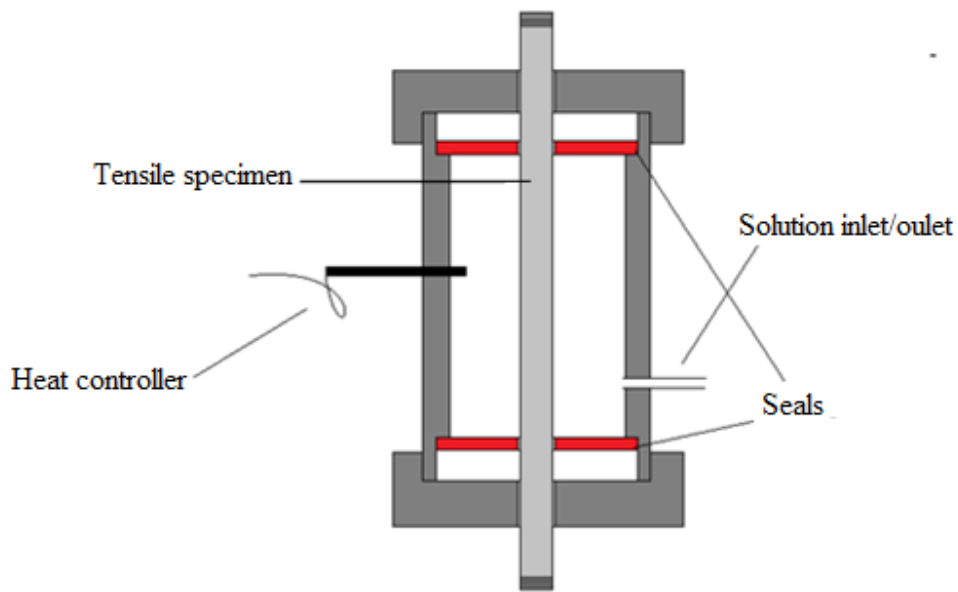


Figure 3.5: SSRT corrosion cell used in the tensile test.

3.4.2 Sample preparation

Slow strain-rate test (SSRT) was used to evaluate the susceptibility of carbon steel to SCC in binary mixtures of ethanol and water. The test specimens, smooth test bars with a circular cross section, were prepared to the dimensions specified in Figure 3.6.

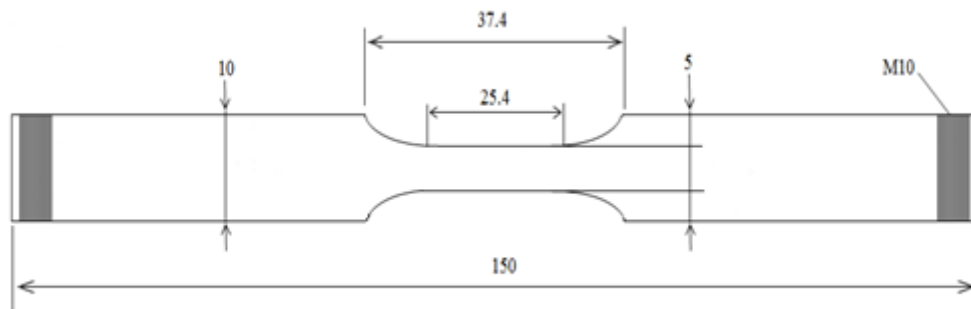


Figure 3.6: Dimensions for SSRT specimens (mm).

The sample shoulders were made quite long, 0.5 times longer than the corrosion cell, to avoid galvanic corrosion between the specimen and the stainless steel grips. The specimens were ground with emery paper of 1200 grit size and the direction of grinding was parallel to the longitudinal axis of the tensile pieces. This direction was maintained to avoid inducing circumferential dents and stress raisers, thus ensuring that any surface cracks perpendicular to the stress would be as a result of SCC. After grinding, the specimens were carefully cleaned with ethanol and dried in a stream of compressed air.

3.4.3 Procedures

i. Calibration of the stepper motor

It is not stress *per se*, but the plastic strain that it produces (Shier et al., 1994) that is responsible for SCC, and the propagation of cracks is dependent on the rate of metal exposure by plastic strain. A slow strain-rate will allow adequate repassivation of the crack tip (Jarvis, 1994) and suppress SCC. On the other hand, a high strain-rate will result in a ductile fracture, as the rate of electrochemical reactions will be too slow to enable repassivation and therefore the propagation of SCC. In this study, strain-rates in order of $10\mu/s$ were chosen.

ii. SSRT

The test environment was made by placing known volumes of water in a measuring cylinder and adding enough ethanol to make a 100 ml solution. The corrosion cell was filled to about 90% volume, and the variation in the load with time was recorded at 15 minute intervals. To avoid trapping water, the corrosion cell was filled with ethanol and soaked for at least 8 hours before the actual test. A baseline test was carried out in air, using a tensile specimen made from ASTM 516. The results obtained in the tests in different ethanol solutions were compared to the results the baseline test.

3.5 Solution characterisation

The properties of the ethanol-water solutions were characterised in terms of acidity, oxygen content and electrical conductivity. The solutions were prepared from analytical grade ethanol and distilled water.

3.5.1 Apparatus

The acidity of the ethanol-water solutions was determined using the Orion Ross Sure-flow combination electrode. The set up used is shown in Figure 3.7.

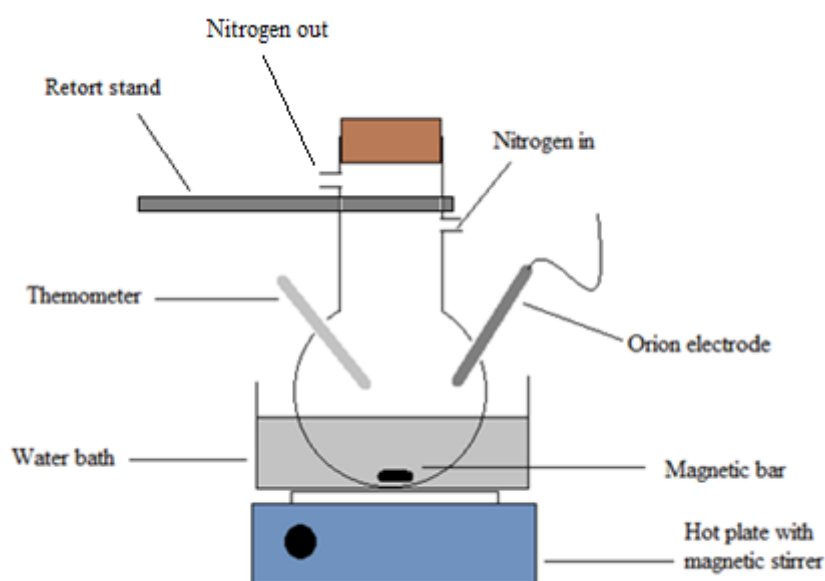


Figure 3.7: Arrangement for measuring pH.

3.5.2 Procedures

i. Water content

To monitor the changes in the water content of ethanol solutions in contact with carbon steel, steel specimens, measuring about 0.3 x 0.5 x 0.3cm were placed in air-tight tubes. The specimens and the tubes were degreased in acetone and dried in a stream of compressed air. The steel coupons were then immersed in the different ethanol-water solutions for a period of 90 days.

Sodium chloride is sparingly soluble in ethanol (at 0.52 g/L), but is highly soluble in water (at 359 g/L). The difference in the solubility is what was used to estimate the water content in solutions containing unknown compositions of ethanol and water. A calibration curve relating solubility as a function of water content was generated using known mixtures of ethanol and water. This curve was then used to determine the composition of unknown mixtures of ethanol and water. The exact procedure is outlined in Appendix A.

ii. Conductivity and dissolved oxygen

The conductivity and dissolved oxygen were measured using probe type meters. In both cases, the readings were noted after 30 s of immersion.

iii. Acidity

The acidity of the ethanol mixtures was monitored by pHe as prescribed in the ASTM D6423 standard. The parameter pHe is a measure of the acid strength of alcohol fuels as defined by the said standard. For each solution sample, successive repeats were taken and the four values whose difference did not exceed 0.29 were averaged. The pHe values were taken before and after immersion.

3.6 Metallographic analysis

The occurrence of SCC was confirmed using a stereo microscope and a scanning electron microscope (SEM).

3.6.1 Apparatus

A TOPCON SM-510 scanning electron microscope made by Oxford Instruments was used. The microscope, with a tungsten filament, was continuously cooled with liquid nitrogen and used a spot size of 10 mm². Analysis was performed with Oxford Link Isis and Link Tetra software operating on a HP work station.

Visual inspection of the fractured and the corroded specimens was performed on a stereo microscope equipped with a Nikon SMZ 745T camera. The camera was operated by NIS Elements (Version 4) imaging software.

3.6.2 Procedures

The carbon steel specimens were stored in a desiccator immediately after slow strain-rate testing. Before examination, the samples were cleaned in acetone in an ultrasonic cleaner for 20 minutes.

3.7 Immersion test

An immersion test was carried out to compliment corrosion rates determined by electrochemical methods. The immersion tests were performed under static conditions at room temperature for a period of 34 days. The dimensions of the test coupons are shown in Figure 3.8.

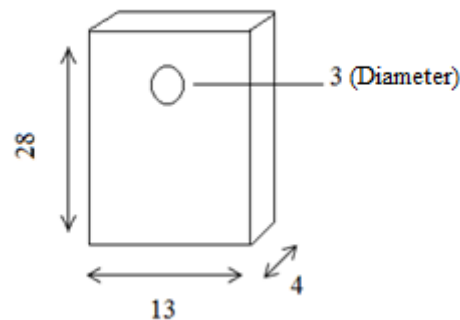


Figure 3.8: Dimensions for the coupons for the immersion tests (mm).

3.7.1 Procedures

The coupons were progressively ground using emery papers of decreasing grit size, from 240 to 1200. They were carefully cleaned in acetone using an ultrasonic cleaner for 20 minutes. The initial mass and dimensions were taken and recorded. The coupons were hung in separate test tubes containing solutions with varying water contents. They were hung using loosely tied cotton threads. The tubes were

sealed to ensure that any oxygen in the solution was from the water. After the immersion period, the specimens were cleaned and their masses recorded.

The corrosion rates were calculated as per Equation 3.3 (Obuka et al, 2012).

$$\text{Corrosion rate} = \frac{K(m_b - m_a)}{\Delta t \times A \times \rho} \dots\dots\dots 3.3$$

K is a constant of unit conversion and its value was quoted as 87.6×10^3 (Van der Merwe, 2011). The parameters m_b and m_a are the mass of the coupon before and after exposure respectively, while A is the exposed area, Δt , the exposure time in hours and ρ is the density of the coupon.

CHAPTER FOUR

RESULTS AND DISCUSSION:

CORROSION CHARACTERISATION

4.1 Introduction

This chapter presents and discusses the results obtained from the electrochemical techniques used to evaluate the corrosion of carbon steel in the various solutions of ethanol and water. The evolution of conductivity, dissolved oxygen and pHe of the different test environments with time was also analysed in the bid to explain the observed corrosion behaviour.

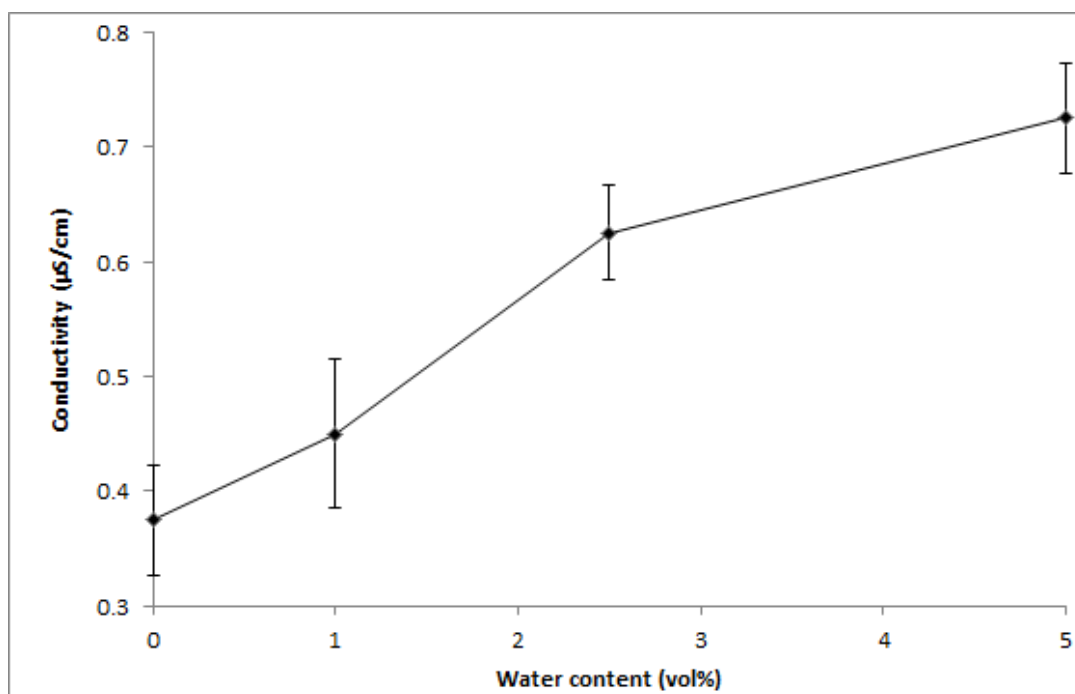
4.2 Solution characterisation

4.2.1 Conductivity

The conductivity of the ethanol-water solutions was measured as per the procedure in Section 3.5.2 and the results are presented in Table 4.1 and Figure 4.1.

Table 4.1: Conductivity before immersion (1 significant figure).

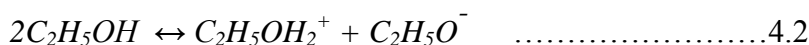
Water content (vol%)	Sample number	Conductivity ($\mu\text{S}/\text{cm}$)	Average conductivity ($\mu\text{S}/\text{cm}$)	Standard deviation	Standard error
0	1	0.3	0.4	0.1	0.04
	2	0.3			
	3	0.5			
	4	0.4			
1	1	0.3	0.5	0.1	0.06
	2	0.5			
	3	0.4			
	4	0.6			
2.5	1	0.5	0.6	0.1	0.04
	2	0.6			
	3	0.7			
	4	0.6			
5	1	0.7	0.7	0.1	0.05
	2	0.8			
	3	0.8			
	4	0.6			

**Figure 4.1:** Conductivity of ethanol-water solutions before immersion.

The increase in water content increased the conductivity of ethanol-water mixtures from 0.4 $\mu\text{S}/\text{cm}$ at 0 vol% water to 0.7 $\mu\text{S}/\text{cm}$ at 5 vol% water. Electrical conductivity in a solution occurs when there are ionisable species in the solution capable of providing mobile ions. The observed conductivity trend could be because of the autoprotolysis of water according to Equation 4.1.



Ethanol is also a protic solvent capable of self-dissociation by Equation 4.2 (Metzge, 2012)



However, the ionic products formed by Equation 4.2 are much fewer as evidenced by the low ion product constant (K_s) shown in Table 4.2.

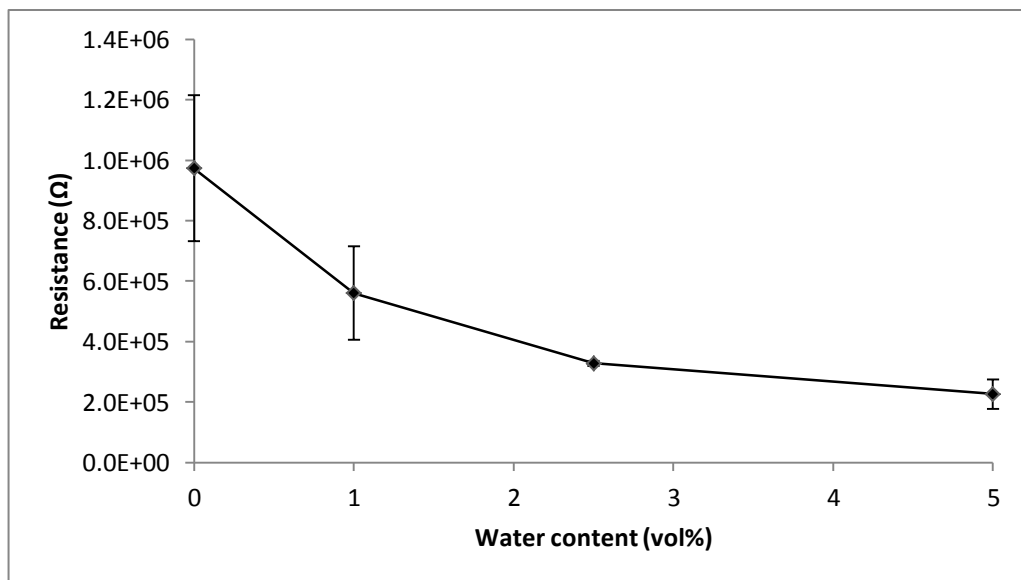
Table 4.2: Ion product of water and ethanol.

Solvent	Ion product (K_s)
$\text{C}_2\text{H}_5\text{OH}$	10^{-19}
H_2O	10^{-14}

The increase in the concentration of ionic products produced by the autoprotolysis of water leads to an increase in the dielectric constant of ethanol (Section 2.2.2) and therefore electrical conductivity. The trend observed in Figure 4.1 is in agreement with surveyed literature (ORNL, 2008; Spitze et al., 2009), and that of the solution resistance as obtained by EIS (Table 4.3 and Figure 4.2).

Table 4.3: Solution resistance as measured by EIS

Sample number	No water	1 vol% water	2.5 vol% water	5 vol% water
1	1.53E+06	9.47E+05	3.60E+05	1.24E+05
2	1.44E+06	4.08E+05	3.17E+05	1.64E+05
3	3.76E+05	7.37E+05	3.27E+05	2.55E+05
4	6.75E+05	6.51E+05	3.16E+05	3.80E+05
5	1.21E+06	4.51E+04	3.15E+05	2.85E+05
6	6.08E+05	5.72E+05	3.35E+05	1.54E+05
Average	9.73E+05	5.60E+05	3.28E+05	2.27E+05
Standard deviation	4.82E+05	3.09E+05	1.74E+04	9.74E+04
Standard error	2.41E+05	1.55E+05	8.68E+03	4.87E+04

**Figure 4.2:** Solution resistance measured by EIS.

Solution resistance is inversely proportional to conductivity. As such, the trend in Figure 4.2 shows an increased conductivity with increase in water content. The electrical conductivity of the solutions was also measured at the end of the immersion period. It was found to be significantly higher than the initial conductivity values. Table 4.4 and Figure 4.3 show the results of the experiment.

Table 4.4: Conductivity after immersion (2 significant figures).

Water content (vol%)	Sample number	Conductivity ($\mu\text{S}/\text{cm}$)	Average conductivity ($\mu\text{S}/\text{cm}$)	Standard deviation	Standard error
0	1	4.2	3.8	0.35	0.18
	2	3.6			
	3	3.4			
	4	3.9			
1	1	7.7	7.6	0.32	0.16
	2	7.7			
	3	7.8			
	4	7.1			
2.5	1	5.4	5.5	0.25	0.13
	2	5.2			
	3	5.8			
	4	5.4			
5	1	5.2	4.9	0.26	0.13
	2	4.7			
	3	4.6			
	4	4.9			

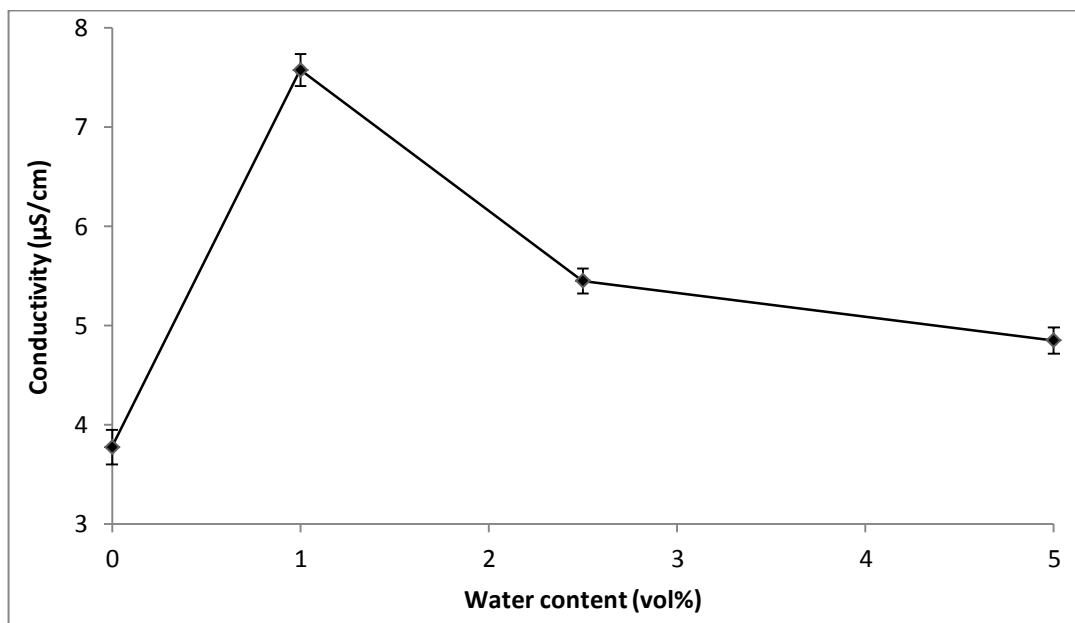


Figure 4.3: Conductivity after 72 hours of immersion.

The observed values were too high to be explained by the autoprotolysis of water, or the increase in the dielectric constant of ethanol with water percentage. As such, the source of this high electrical conductivity was not the increasing water content, but rather the presence of corrosion products. The major corrosion product was likely to contain ferric ions, which have a high mobility and electrical conductivity.

Besides being an indication of the risk of corrosion in a solution, electrical conductivity can be a reflection of the concentration of the conducting ions in the solution (Codd et al., 1970; Spitze et al., 2009). From Figure 4.3, the conductivity of the solution with 1 vol% water had the highest conductivity of 7.6 $\mu\text{S}/\text{cm}$, implying the highest concentration of ferric ions. The extent of corrosion in this solution would be expected to be severe.

4.2.2 Dissolved oxygen

The amount of oxygen in a solution generally determines its potential as a corrosive medium. The effect of water on the oxidising strength of ethanol was analysed by monitoring the amount of dissolved oxygen in the solutions before and after immersion (as per Section 3.5.2). The results are presented in Figure 4.4 and Tables 4.5 and 4.6. Table 4.7 compares the dissolved oxygen before and after immersion.

Table 4.5: Dissolved oxygen before immersion.

Water content (vol%)	Sample number	Dissolved oxygen (mg/L)	Average dissolved oxygen (mg/L)	Standard deviation	Standard error
0	1	5.85	6.00	0.15	0.08
	2	6.17			
	3	6.09			
	4	5.90			
1	1	6.12	6.09	0.28	0.14
	2	6.46			
	3	5.81			
	4	5.95			
2.5	1	6.20	6.11	0.15	0.08
	2	6.16			
	3	5.88			
	4	6.18			
5	1	6.00	6.45	0.52	0.26
	2	6.82			
	3	6.98			
	4	6.00			

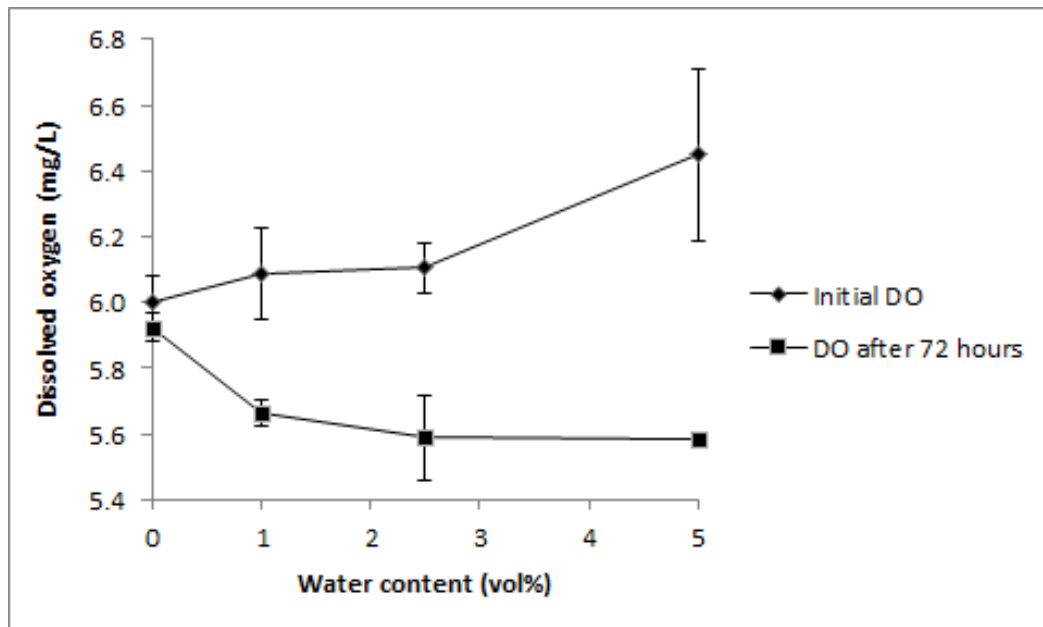


Figure 4.4: Variation of dissolved oxygen (DO) with time and water content.

Table 4.6: Dissolved oxygen after 72 hours of immersion.

Water content (vol%)	Sample number	Dissolved oxygen (mg/L)	Average dissolved oxygen (mg/L)	Standard deviation	Standard error
0	1	6.03	5.93	0.09	0.04
	2	5.90			
	3	5.82			
	4	5.95			
1	1	5.76	5.66	0.08	0.04
	2	5.59			
	3	5.69			
	4	5.61			
2.5	1	5.58	5.59	0.03	0.01
	2	5.60			
	3	5.62			
	4	5.56			
5	1	5.55	5.58	0.04	0.02
	2	5.63			
	3	5.54			
	4	5.61			

Table 4.7: Comparison of dissolved oxygen before and after immersion.

Water content (vol%)	Initial dissolved oxygen (mg/L)	Dissolved oxygen after 72 hours (mg/L)	Percentage difference (%)
0	6.00	5.93	1.17
1	6.09	5.66	7.06
2.5	6.11	5.59	8.51
5	6.45	5.58	13.49

Before immersion, there was an increase in the quantity of dissolved oxygen with increase in water added. The trend observed was expected, since water contains dissolved oxygen. As such, an increase in water will result in an increase in the oxidising strength of ethanol-water mixtures. However, the content of dissolved oxygen decreased with time, with the dissolved oxygen in ethanol containing 5 vol% water decreasing by as much as 13% after 72 hours of immersion.

The concentration of oxygen in undiluted ethanol changed by only 0.078 mg/L over the 72 hours of immersion. This slight change could be due to the fact that anhydrous ethanol is hygroscopic, and the absorbed water ensures a constant replenishment of dissolved oxygen. It is likely that the presence of water in ethanol reduced its affinity for water vapour, and therefore its ability to replenish any oxygen consumed by corrosion processes.

Perry (1999) showed that oxidising substances do not always accelerate corrosion processes, but may retard them if the oxidising substance can form and preserve a protective film on the material's surface. The ability of the oxidising agent to preserve a protective film depends primarily on the rate at which it is replenished at the corrosion interface. A limited supply of the oxidising species can be detrimental in so far as maintaining a passive state is concerned. Given this, the poor replenishment of oxygen in ethanol-water mixtures with increased water contents would mean reduced ability to repair any passive films broken down, either by localised dissolution or by mechanical rupture.

4.2.3 Acidity

The acidity of a solution can be used to qualify its potential as a corrosive medium. In ethanol, this acidity is quantified by pHe which is, as is the case with aqueous solutions, the negative logarithm of the activity of hydrogen ions in the ethanol solution. On the pHe scale, 9.6 at 25°C is neutral, and a pHe of 6 is considered highly acidic (Kane et al., 2004; Spitzer et al., 2009). Tables 4.8 and 4.9 present the results obtained in the experiment.

Table 4.8: pHe measurements before immersion.

Sample number	No water	1vol% water	2.5vol% water	5vol% water
1	5.55	5.66	5.85	6.20
2	5.39	6.03	6.67	5.92
3	6.46	6.17	6.44	5.86
Mean	5.80	5.95	6.32	5.99
Standard deviation	0.58	0.26	0.42	0.18
Standard error	0.29	0.13	0.21	0.09

Table 4.9: pHe measurements after 72 hours of immersion.

Sample number	No water	1vol% water	2.5vol% water	5vol% water
1	5.43	5.74	6.20	6.10
2	5.64	5.83	5.12	5.55
3	5.20	5.33	5.55	5.65
Mean	5.42	5.63	5.62	5.77
Standard deviation	0.22	0.27	0.54	0.29
Standard error	0.11	0.13	0.27	0.15

Figure 4.5 shows the pHe of the ethanol solutions before and after immersion.

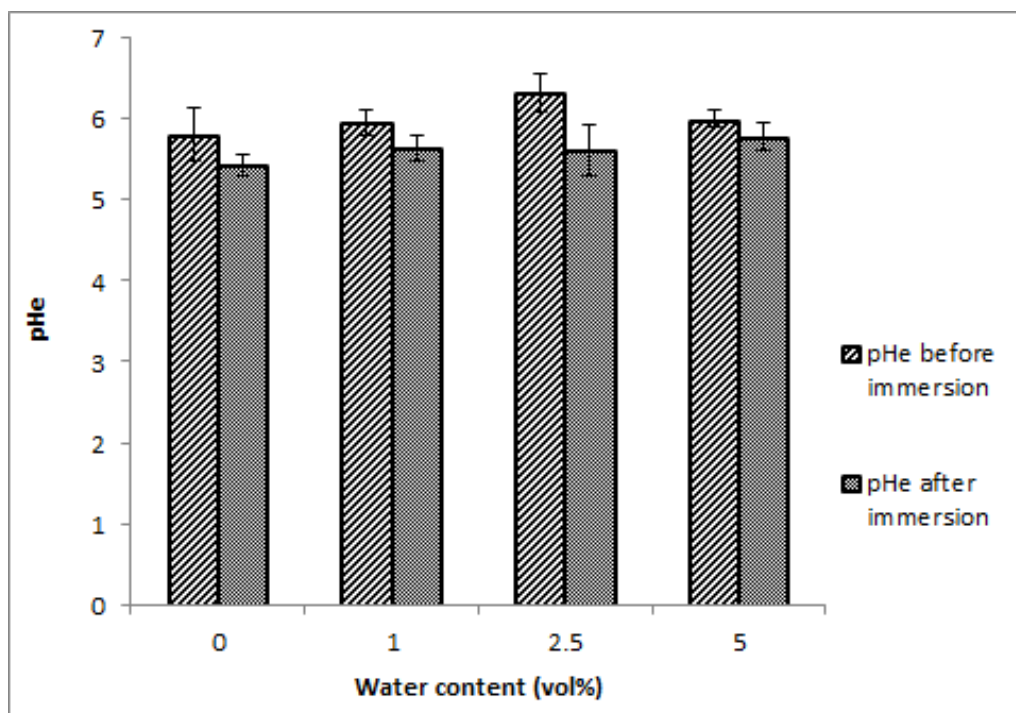


Figure 4.5: Variation of pHe with water content.

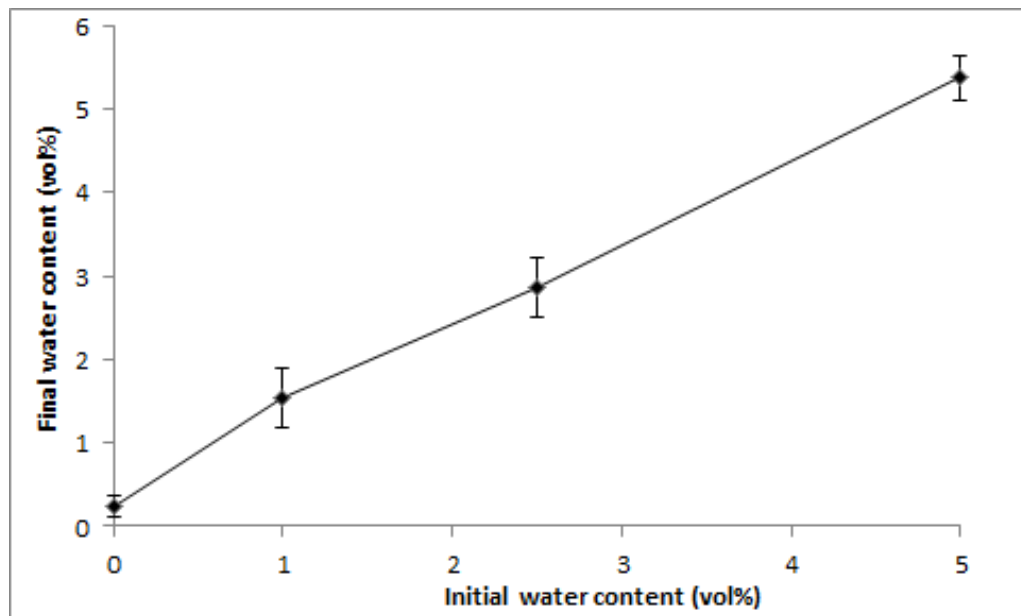
The increase in water does not seem to significantly affect the acidity of the ethanol-water mixtures. The pHe of anhydrous ethanol was found to be about 5.80. Increasing water content by 5 vol% increased the pHe slightly to 5.99.

After 72 hours, there was a decrease in the pHe values, implying that the solutions became more acidic with time. This is in agreement with some researchers that ethanol has a tendency to degrade over time (Agarwal, 2007; Lou et al., 2009; Lou & Singh, 2011). The increase in acidity with time means a decrease in the ability to form protective surface films in the given solutions.

Acetic acid has been proposed as one of the products of ethanol degradation (Newman, 2008; Lou et al., 2009). The acetic acid is likely to be produced by Equation 2.5 shown in Section 2.2.2. This reaction also produces water. As such, the decrease in pHe (i.e. the increase in acidity) should be accompanied by an increase in water content. Table 4.10 and Figure 4.6 confirm this.

Table 4.10: Estimated water content after 90 days of immersion.

Initial water content (vol%)	Sample number	NaCl solubility (g/50ml)	Estimated water content (vol%)	Average water content (vol%)	Standard deviation	Standard error
0	1	0.075	0.189	0.239	0.237	0.137
	2	0.083	0.497			
	3	0.071	0.032			
1	1	0.100	1.123	1.533	0.620	0.358
	2	0.103	1.230			
	3	0.133	2.246			
2.5	1	0.164	3.063	2.864	0.608	0.351
	2	0.175	3.347			
	3	0.131	2.181			
5	1	0.248	5.274	5.369	0.479	0.276
	2	0.262	5.888			
	3	0.234	4.945			

**Figure 4.6:** Water content after 90 days as a function of initial water content.

There was a notable increase in water in all the solutions studied. The oxygen dissolved in the initial water may have facilitated the oxidation reaction in

Equation 2.5 to produce more water. This was true for solutions with initial water contents of 1, 2.5 and 5 vol%.

Agarwal (2007) indicated that metals may undergo dry corrosion in ethanol, a corrosion process attributed to the ethanol molecule and its polarity. Broadly speaking, corrosion is a consequence of the reduction of oxygen or an oxidising species. That anhydrous ethanol can support dry corrosion means that ethanol contains some dissolved oxygen as illustrated in Figure 4.4. This oxygen could have enabled the oxidation of ethanol and caused an increase in water content. The observed trends mean that even in the absence of ambient oxygen and humidity, ethanol will contain some percentage of water.

4.3 Passivation tendencies

The evolution of open circuit potential (OCP) with time was used to evaluate the general corrosion behaviour of carbon steel in ethanol-water mixtures. The data obtained over the 72 hours of experimentation are presented in Table 4.11 and Figure 4.7.

Table 4.11: Variation of OCP with time.

Time (h)	OCP vs Ag/AgCl EtOH (mV)			
	No water	1vol% water	2.5vol% water	5vol% water
0	201	141	90	59
12	282	217	224	209
24	293	223	214	145
36	308	169	205	199
48	290	158	174	170
60	311	167	158	161
72	314	201	166	167

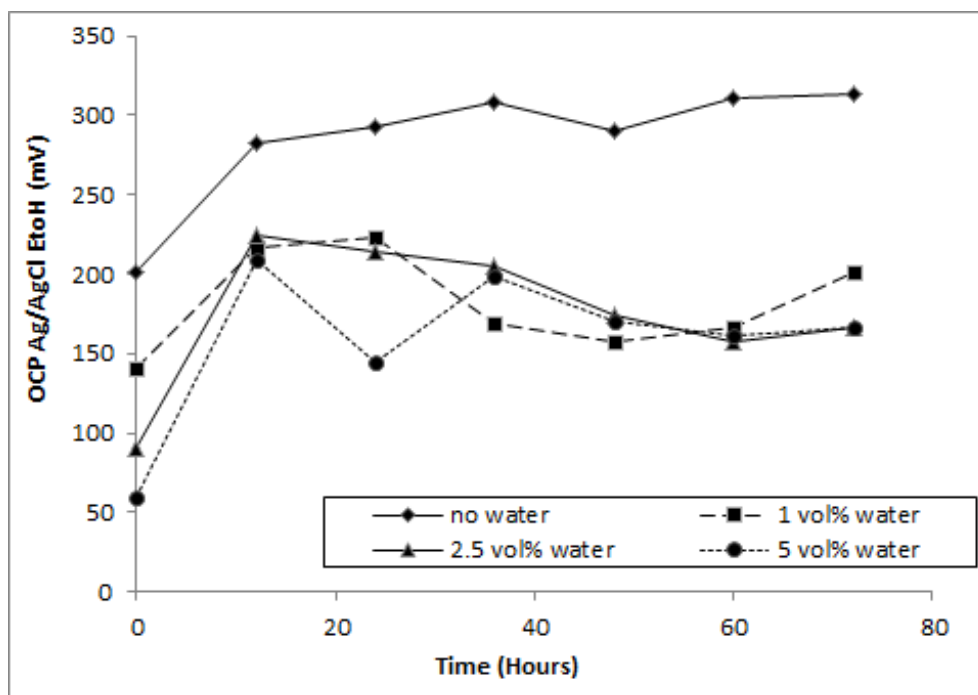


Figure 4.7: Evolution of OCP with time for different ethanol-water solutions.

In the solutions studied, the OCP values exhibited a general positive increase over time. For all the cases, the shift was quite rapid in the first 12 hours, indicative of a rapid formation of passive films. The increase in OCP was most rapid in solutions with 5 vol% water; increasing at a rate of about 12.5 mV/h in the first 12 hours compared with 6.33 mV/h in anhydrous ethanol in the same time interval. It was noted in Section 4.2.2 that the presence of water in ethanol increased the amount of oxygen in the solution, the highest quantity being associated with 5 vol% water. This high oxygen content could be responsible for the observed trend.

For ethanol with no water, the OCP values increased at a rather slow steady rate in the next 60 hours. The rate can be attributed to slow reaction rates, and is associated with a relatively stable passive layer. In the solutions with 1, 2.5 and 5 vol% water, the OCP fluctuated with time in the next 60 hours of the experiment owing to dissolution-repassivation processes. This trend suggests that the presence of water resulted in higher corrosion rates. It also points to the presence of unstable surface films. The film formed in the solution with 5 vol% water

appeared to be the least stable, resulting in a very sharp drop and rise of OCP between 12 and 36 hours. The limited supply of oxygen discussed in Section 4.2.2 could be responsible for the unstable passive film in these solutions.

The thickness of the passive films was characterized using double layer capacitance (C_{dl}) obtained by EIS. The results are given in Table 4.12 and Figure 4.8.

Table 4.12: Double layer capacitance

Sample number	No water	1 vol% water	2.5 vol% water	5 vol% water
1	2.28E-06	2.51E-05	2.44E-07	3.31E-05
2	1.85E-06	1.63E-05	1.69E-05	3.56E-06
3	1.70E-06	2.26E-05	1.73E-05	3.37E-06
4	4.58E-06	2.13E-05	1.61E-05	2.58E-05
5	1.61E-06	2.56E-05	1.76E-05	2.63E-05
6	1.60E-06	4.86E-06	1.68E-05	3.15E-06
Average	2.27E-06	1.93E-05	1.42E-05	1.59E-05
Standard deviation	1.16E-06	7.82E-06	6.84E-06	1.40E-05
Standard error	5.80E-07	3.91E-06	3.42E-06	6.98E-06

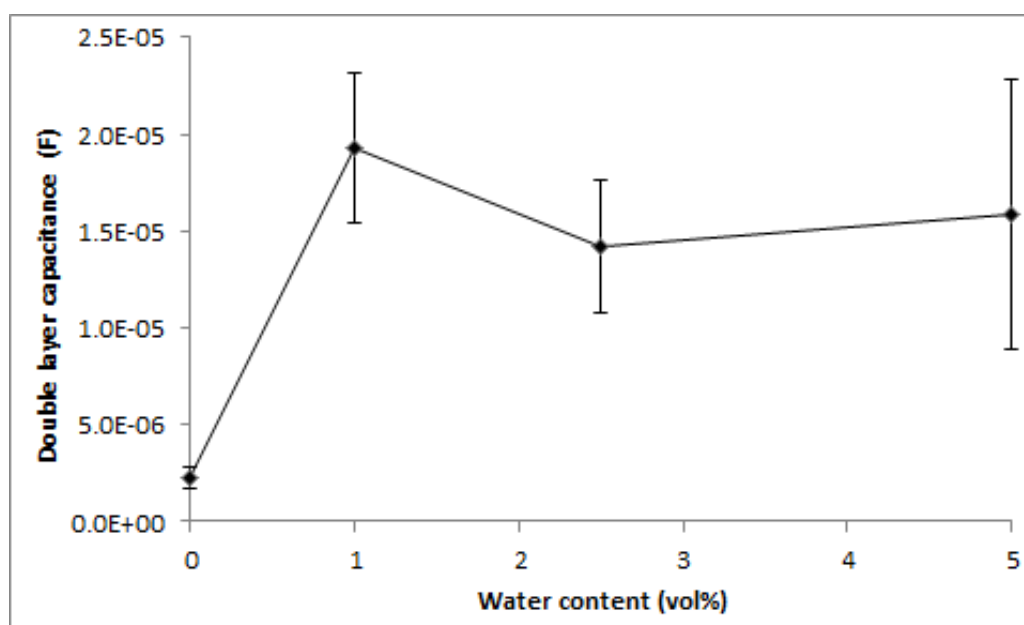


Figure 4.8: Double layer capacitance (C_{dl}) as a function of water content.

The parameter C_{dl} is related to film thickness by Equation 2.12 in Section 2.5.2. According to this equation, C_{dl} is inversely proportional to film layer thickness. In Figure 4.8, the carbon steel sample in anhydrous ethanol shows the lowest C_{dl} value (2.27 μF), indicating the presence of a relatively thick surface film. This is consistent with the slow reaction rates suggested by the OCP values. Passivation is in its own right a corrosion process resulting from the consumption of oxygen. The formation of surface films in anhydrous ethanol solutions is by dry corrosion.

The ethanol solution with 1 vol% water is associated with the highest C_{dl} value, implying that the surface film produced in this solution was quite thin, in fact, thinner than that formed in solutions containing 2.5 and 5 vol% water. This observation could mean that higher corrosion rates were associated with ethanol solutions with 1 vol% water. It also implies that the rates of anodic dissolution are higher than rates of film repair, thus minimising the susceptibility of SCC in the solution.

4.4 Corrosion mechanism

EIS was used to investigate the corrosion mechanism of the carbon steel in ethanol-water mixtures. The Nyquist and Bode (phase) plots are presented in Figure 4.9.

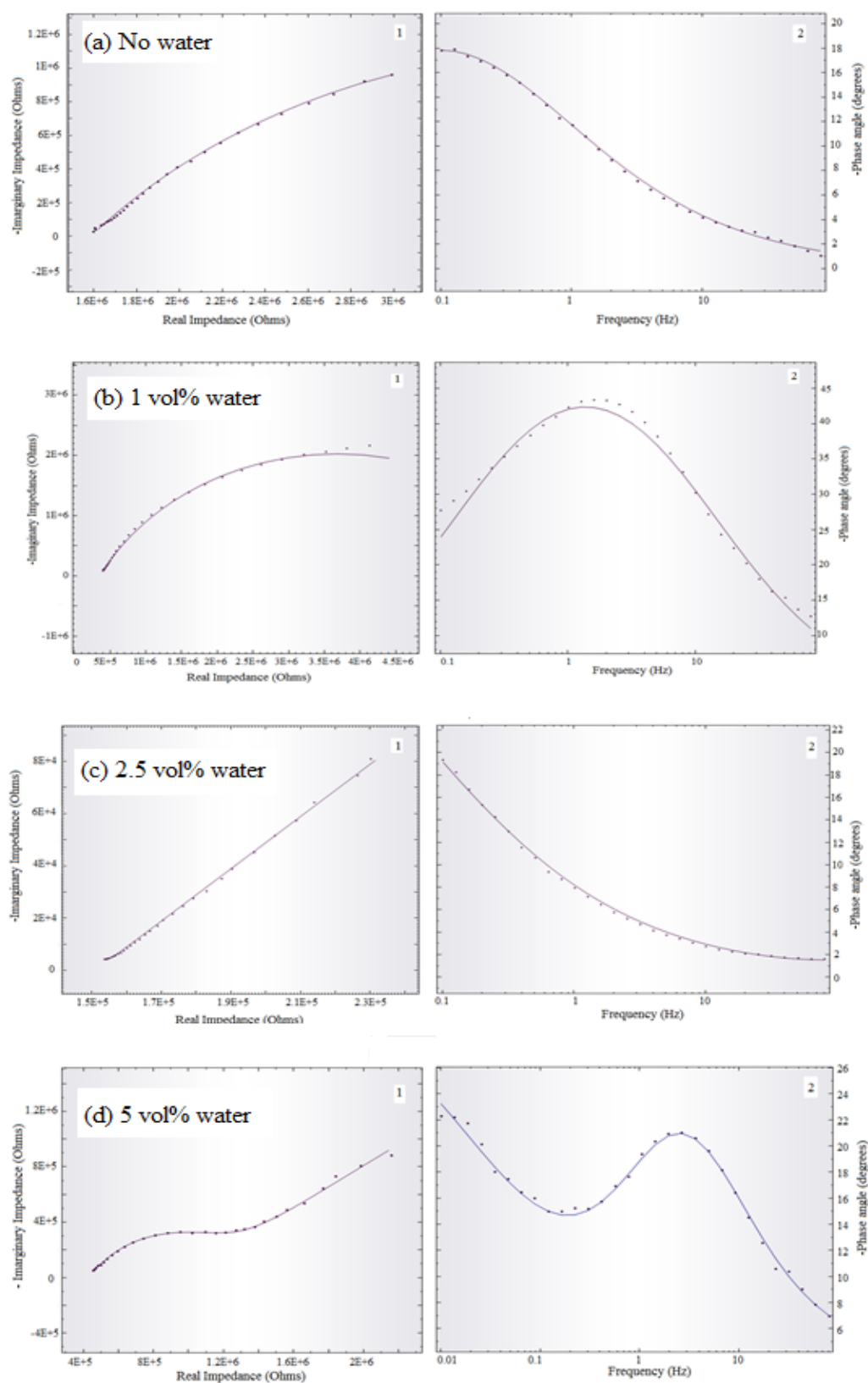


Figure 4.9: The Nyquist (left) and Bode (right) plots for carbon steel in different ethanol-water solutions.

The Nyquist plot in the ethanol solution containing no water (Figure 4.9 (a)) shows the beginning of a semicircle, indicating a reaction sequence that is charge transfer controlled. This should be expected, given the high resistivity associated with this solution presented in Figures 4.1 and 4.2. The semicircle appears to have a considerably large radius, implying a large value for the polarisation resistance. Polarisation resistance is due to the formation of insoluble protective films (Codd et al., 1970) and a large resistance is indicative of negligible corrosion rates.

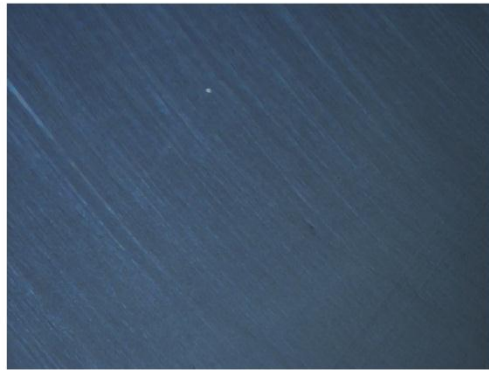
In the solution with 1 vol% water, the Nyquist plot, Figure 4.9 (b), is also a semicircle but with a smaller radius, suggesting higher corrosion rates. While the Nyquist plot suggests a charge transfer controlled reaction sequence, the Bode plot (Figure 4.9 (b) right) indicates a corrosion process under mixed control. The corrosion process is not only dependent on the resistivity of the solution, but also on the mass transport of oxygen to the corrosion surface. This is consistent with the suggestion made in Section 2.2.2 that the presence of water in ethanol markedly reduces the diffusion rate of oxygen in the reaction surface.

An increase in water content to 2.5 vol% changes the shape of the Nyquist plot (Figure 4.9 (c)) to a straight line with a slope of about 0.93. The shape of the plot means that the corrosion reaction in the solution is diffusion-controlled. The Warburg impedance, represented by the slope of the plot is almost one, indicating active corrosion.

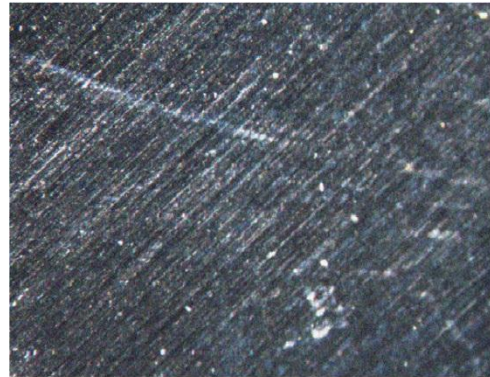
The Nyquist plot in Figure 4.9(d) shows a depressed semi-circle at high frequencies and a straight line at low frequencies, indicating a corrosion process that is under mixed control: charge transfer at high frequencies and diffusion at low frequencies. The depression on the circle could be due to a lack of homogeneity of the electrode surface, perhaps inhomogeneity brought about by local attack.

Post-test examination, by use of a stereomicroscope, was used to confirm the suggested corrosion mechanisms. Figure 4.10 presents the results of the visual inspection of the carbon steel specimens exposed to the different ethanol-water

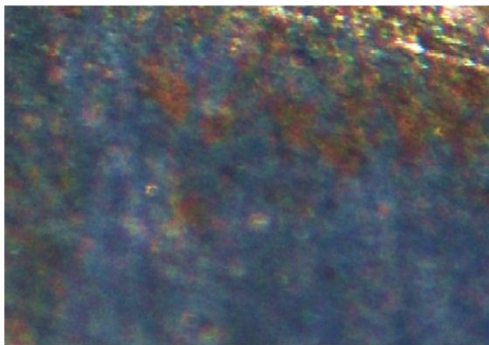
mixtures for 72 hours. The corroded samples were compared to an un-etched un-corroded baseline sample (Figure 4.10(a)).



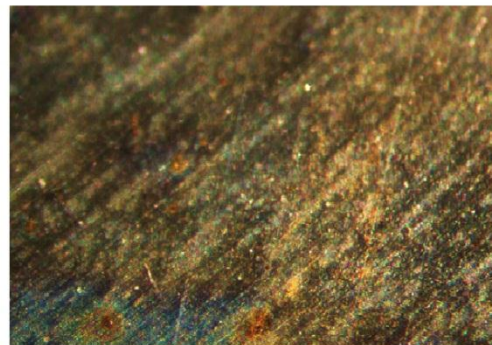
(a) Baseline sample



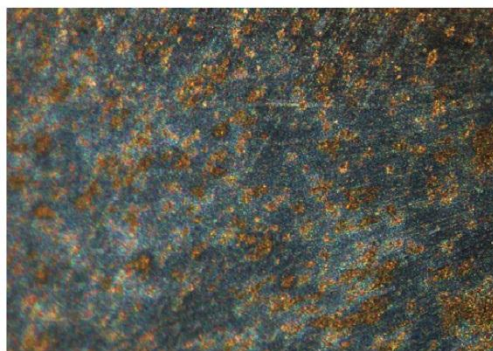
(b) No water



(c) 1 vol% water



(d) 2.5 vol% water



(e) 5 vol% water

Figure 4.10: Micrographs of the carbon steel after 72 hours of immersion.

Figure 4.10 (b) does not exhibit notable corrosion yet when compared to the carbon steel before exposure; it shows a considerable extent of tarnish. It is possible that this tarnish was due to the presence of a passive film. The steel specimens exposed to 1, 2.5 and 5 vol% water exhibited various degrees of localized attack. Since localized attack occurs on a film covered metal surface, this observation implies that carbon steel does passivate in these solutions and supports the rapid film formation deduced from Figure 4.7. Thompson and his colleagues (1988) showed that in some metals local attack is a consequence of diffusion-controlled behavior. The observed localized attack in Figures 4.10 (c), (d) and (e) is consistent with the diffusion-controlled behavior predicted from Figure 4.9 and indicates poor repassivation kinetics in these solutions. The extent of corrosion is more severe in the solutions containing 1 and 5 vol% water, and in both cases the corrosion reaction sequence was predicted to be under mixed control.

4.5 Corrosion rates

Corrosion rates were evaluated by the use of LPR, EIS and weight loss tests. Table 4.13 and Figure 4.11 show the corrosion potentials for carbon steel in different ethanol-water mixtures.

Table 4.13: Corrosion potential of carbon steel in ethanol-water solutions.

Water content (vol%)	Ecorr 1 (mV)	Ecorr 2 (mV)	Ecorr 3 (mV)	Ecorr 4 (mV)	Average Ecorr (mV)	Standard Deviation	Standard error
0	261	266	242	230	249.75	16.74	8.37
1	218	225	217	239	224.75	10.14	5.07
2.5	183	178	195	188	186.00	7.26	3.63
5	154	169	201	193	179.25	21.64	10.82

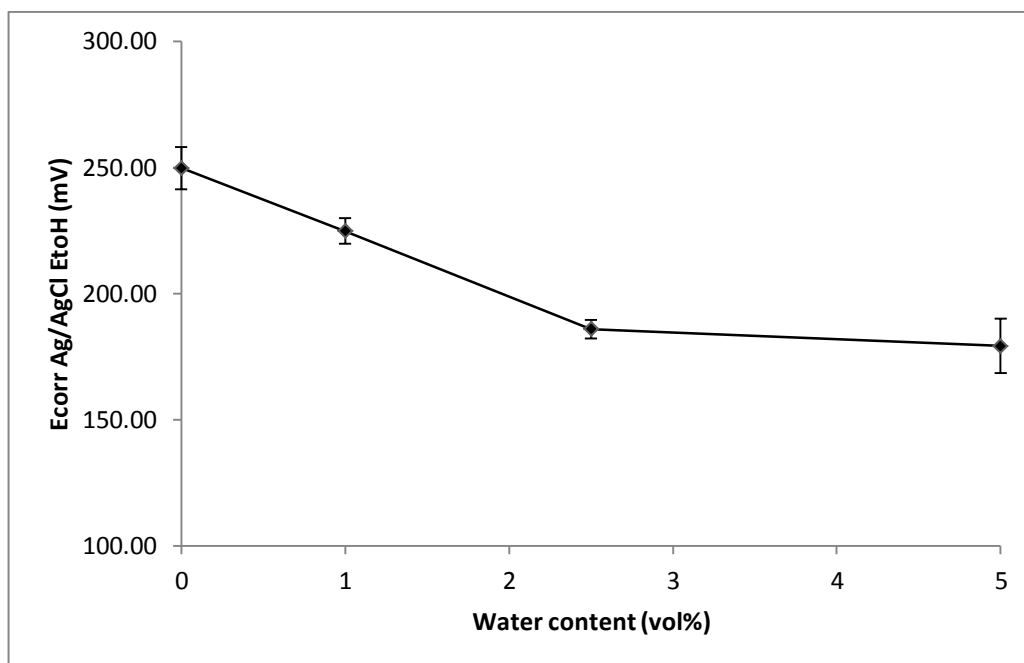


Figure 4.11: Variation in corrosion potential with water content.

Figure 4.11 shows that the addition of water caused a shift in the corrosion potential towards less noble values. This suggests that adding water to ethanol makes the solution more corrosive and the corrosion processes more spontaneous. The reasons for these observations have already been discussed in Section 4.2. The reduction in corrosion potential with increased water content also implies that the corrosion of carbon steel in hydrated ethanol arises from reactions of the metal with the aqueous component of the solution.

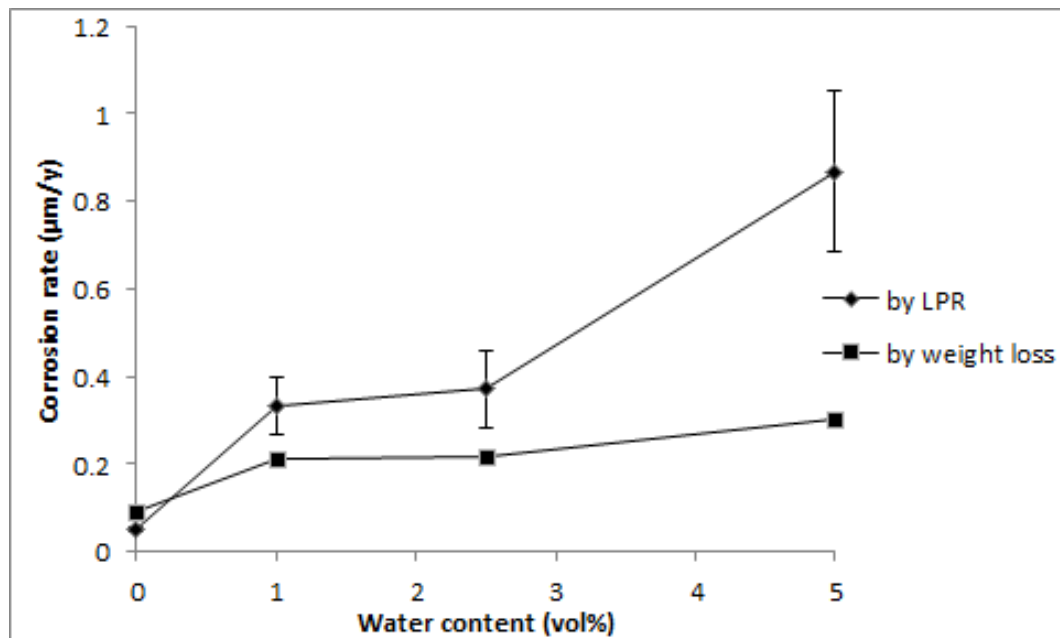
Based on the arguments raised above, it should be expected that solutions with higher water content would support higher corrosion rates. Figure 4.12 compares the corrosion rates obtained by LPR and weight loss. Corrosion rates by LPR were calculated in accordance with ASTM G102-89 (Reapproved 1999).

Table 4.14: Corrosion rates measured by LPR.

Sample number	No water	1 vol% water	2.5 vol% water	5 vol% water
1	0.0477	0.4618	0.2130	0.8156
2	0.0426	0.2054	0.5622	1.2556
3	0.0617	0.3314	0.3413	0.5313
Average corrosion rate ($\mu\text{m/y}$)	0.0507	0.3329	0.3721	0.8675
Standard deviation	0.0099	0.1282	0.1766	0.3649
Standard error	0.0049	0.0641	0.0883	0.1825

Table 4.15: Corrosion rates by weight loss.

Water content (vol%)	Mass before exposure (g)	Mass after exposure (g)	Area exposed (mm^2)	Corrosion rate ($\mu\text{m/y}$)
0	11.5220	11.5219	15.0259	0.0910
1	8.8463	8.8461	12.8565	0.2127
2.5	8.4659	8.4657	12.5863	0.2173
5	17.7865	17.7862	13.5470	0.3028

**Figure 4.12:** Corrosion rates estimated by LPR and weight loss.

It is evident that the corrosion rates measured using LPR and weight loss are not in perfect agreement. Nevertheless, they both show that an increase in water content results in an increase in corrosion rates. The corrosion rates were quite low: in a solution with 5 vol% water, the corrosion rates of carbon steel were found to be $0.303 \mu\text{m/y}$ and $0.868 \mu\text{m/y}$ by weight loss and LPR respectively. This shows that carbon steel is resistant to corrosion in ethanol solutions with up to 5 vol% water.

The observed corrosion rates are supported by the trend in phase angles measured by EIS at the frequency of 0.01 Hz, as shown in Figure 4.13.

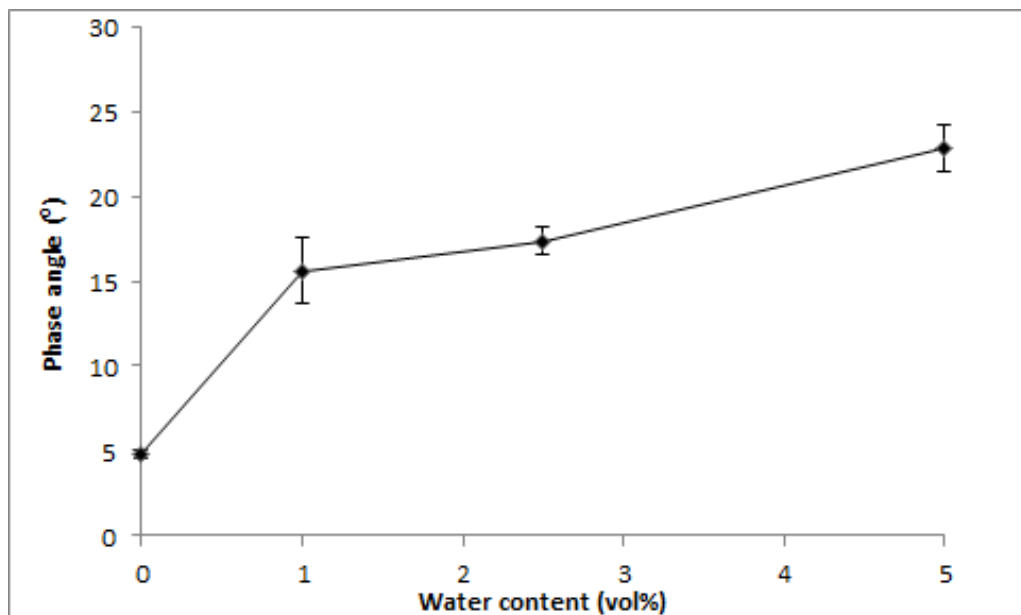


Figure 4.13: Variation of phase angle with water content.

The use of low frequencies allows electrode surface properties to be observed (Sherratt, 1992). To analyse the corrosion rates the phase angles at the lowest frequency (0.01Hz) were recorded. According to Thompson & Lawson (1999), an increase in phase angle at the lowest frequency indicates an increase in corrosion rates. Figure 4.13, shows that the phase angle tended away from zero with increase in water content indicating a reduced corrosion resistance with higher water concentrations.

CHAPTER FIVE

RESULTS AND DISCUSSION:

SLOW STRAIN-RATE TESTING

5.1 Introduction

This chapter details the results from the failure analysis of tensile specimens subjected to slow strain-rate testing (SSRT). Micrographs were taken using both the stereomicroscope and the scanning electron microscope (SEM) to confirm and qualify the occurrence of SCC.

5.2 Characterisation of the carbon steel

For the metallographic characterisation of the carbon steel, two specimens perpendicular to each other were prepared. The micrographs of the specimens are presented in Figure 5.1.

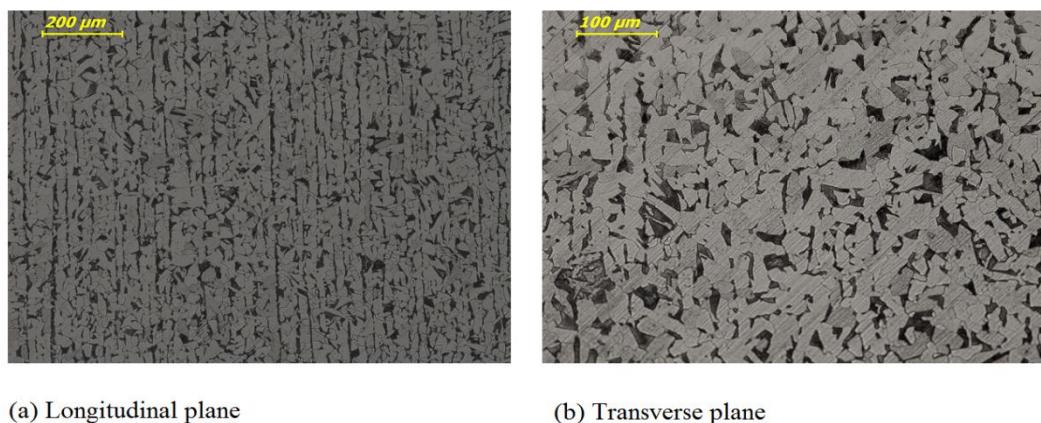


Figure 5.1: Microstructure of the steel showing elongated bands of ferrite and pearlite grains. 2% nital etch.

The major constituent in the steel was ferrite, shown here as light coloured regions. Remnants of scratches (Figure 5.1 (b)) were seen in these light coloured areas, confirming the presence of the softer ferrite phase. Patches of the darker harder pearlite appear at the ferrite grain boundaries. In Figure 5.1 (a), the ferrite grains appeared as elongated bands running parallel to the rolling direction, which is expected in rolled material.

5.3 SCC susceptibility

Slow strain-rate tests were carried out in ethanol solutions with known quantities of water as described in Section 3.4.3. Measures of ductility, expressed as percent elongation and percent area reduction, are presented in Table 5.1 and Figure 5.2. A detailed description of these parameters is given in Appendix B.

Table 5.1: Percent elongation and area reduction.

Water content (vol%)	Original length, l_o (mm)	Final length, l_f (mm)	Percent elongation (%)	Original diameter, D_o (mm)	Final diameter, D_f (mm)	Percent area reduction (%)
Baseline	25.6	31.7	23.8	5.0	2.8	69.5
0	26.0	32.0	23.1	5.0	3.1	61.6
1	26.0	31.3	20.4	5.0	3.0	64.0
2.5	26.0	30.5	17.3	5.0	3.4	52.7
5	25.5	32.0	25.5	5.0	3.0	64.0

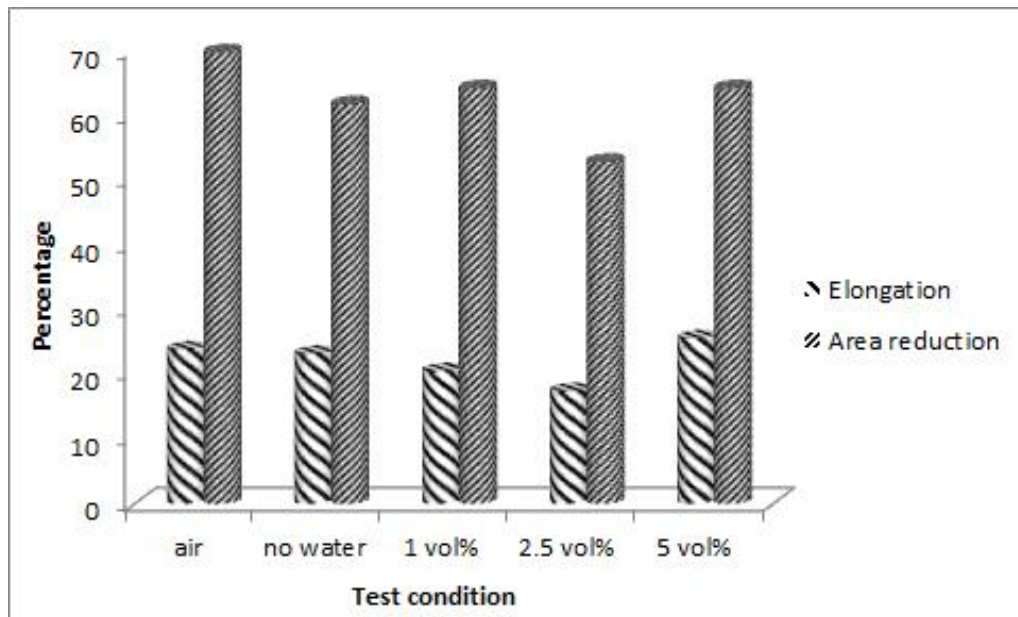


Figure 5.2: Percentage elongation and area reduction as a function of water content.

In air, the carbon steel exhibited an elongation and area reduction of about 24 and 70% respectively. These values indicate that the steel specimen had good ductility which may be attributed to the low carbon and phosphorus content in the metal (Table 3.1).

The carbon steel specimen in ethanol with 2.5 vol% water showed significantly reduced ductility with elongation of not more than 18% and area reduction of about 53%. According to Lou et al. (2009), reduced ductility is an indication of high SCC susceptibility. Given this and the results presented in Figure 5.2, the susceptibility to SCC increased with an increase in water content up to 2.5 vol%. A further increase in water had the effect of reducing SCC susceptibility.

Environments that tend to promote SCC are those in which corrosion is localised (Robertson, 1956; Karpenko & Vasilenko, 1979; NPL, 2000). As shown in Chapter 4, ethanol solutions with 1 and 2.5 vol% water supported localised attack. The reduced rates of oxygen replenishment to the corroding interface resulted in low repassivation kinetics in these solutions. This would lead to a higher susceptibility to SCC.

At 5 vol% water, there was a notable increase in ductility, implying a reduction in the risk of SCC. This observation is consistent with two separate studies (Lou et al, 2009; Goodman & Singh, 2011), which showed low SCC susceptibility of carbon steel in ethanol with 5 vol% water. In Section 4.2.2, it was shown that ethanol solutions with 5 vol% water exhibited very low diffusion rates of oxygen. It is therefore possible that in these solutions, the rates of metal dissolution were considerably higher than those of film repair, thus eliminating SCC.

The NACE standard TM0111-2011 uses SCC ratios to evaluate SCC susceptibility. SCC ratios are the ratios of the tensile strength and plastic elongation values obtained in the test environment to the values obtained from the baseline test. Table 5.2 summarises the classification of fractures using SCC ratios.

Table 5.2: Predicting SCC susceptibility from SCC ratios (derived from NACE TM0111-2011).

Class	SCC ratio values	SCC susceptibility
1	1	Normal ductile behaviour: No SCC
2	Slightly reduced from 1	Borderline SCC behaviour
3	Substantially reduced from 1	Substantial SCC behaviour

The determination of SCC ratios was based on percent elongation as presented in Figure 5.3.

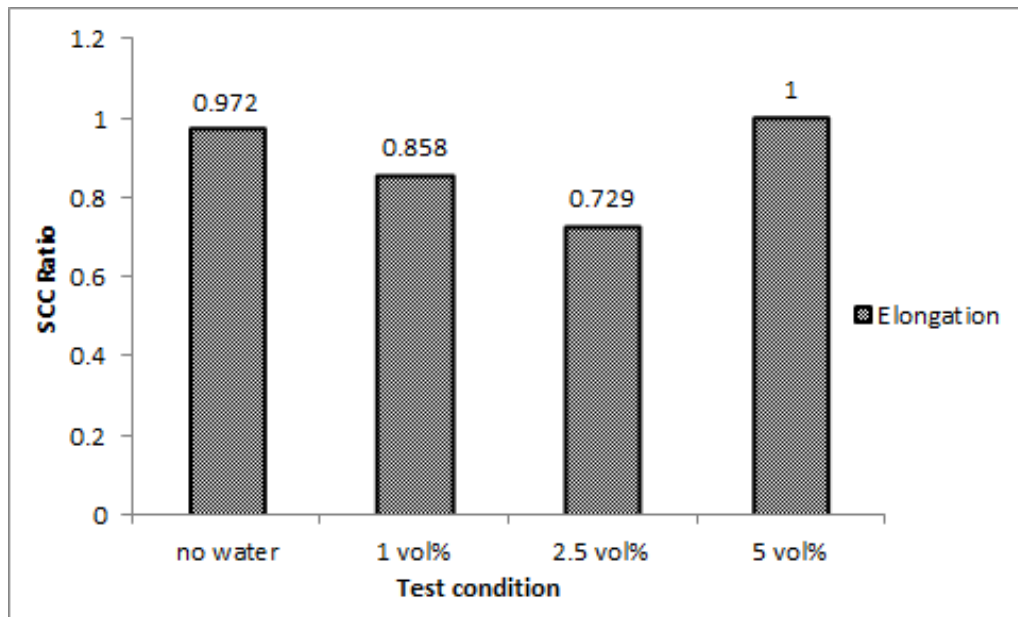


Figure 5.3: Variation of SCC ratios with water content.

According to TM0111-2011, carbon steel specimens in ethanol solutions with no water and with 1 vol% water exhibited borderline SCC behaviour. The specimen in ethanol containing 2.5 vol% water had a SCC ratio of 0.729. This value indicates a greater probability of SCC behaviour. The tensile specimen in the solution with 5 vol% had a ratio of 1, an indication of normal ductile behaviour. This is consistent with the high elongation percentage for the specimen in Figure 5.2.

SCC is accompanied by a reduction in fracture toughness. Young (1989) highlighted that the energy absorbed during fracture affords a criterion for comparing the toughness of different materials. This energy is directly proportional to fracture toughness; the higher the energy, the tougher the material. In this work, the energy was estimated from the area under the stress-strain curves in Figure 5.4 using the Trapeziodal method (Appendix B).

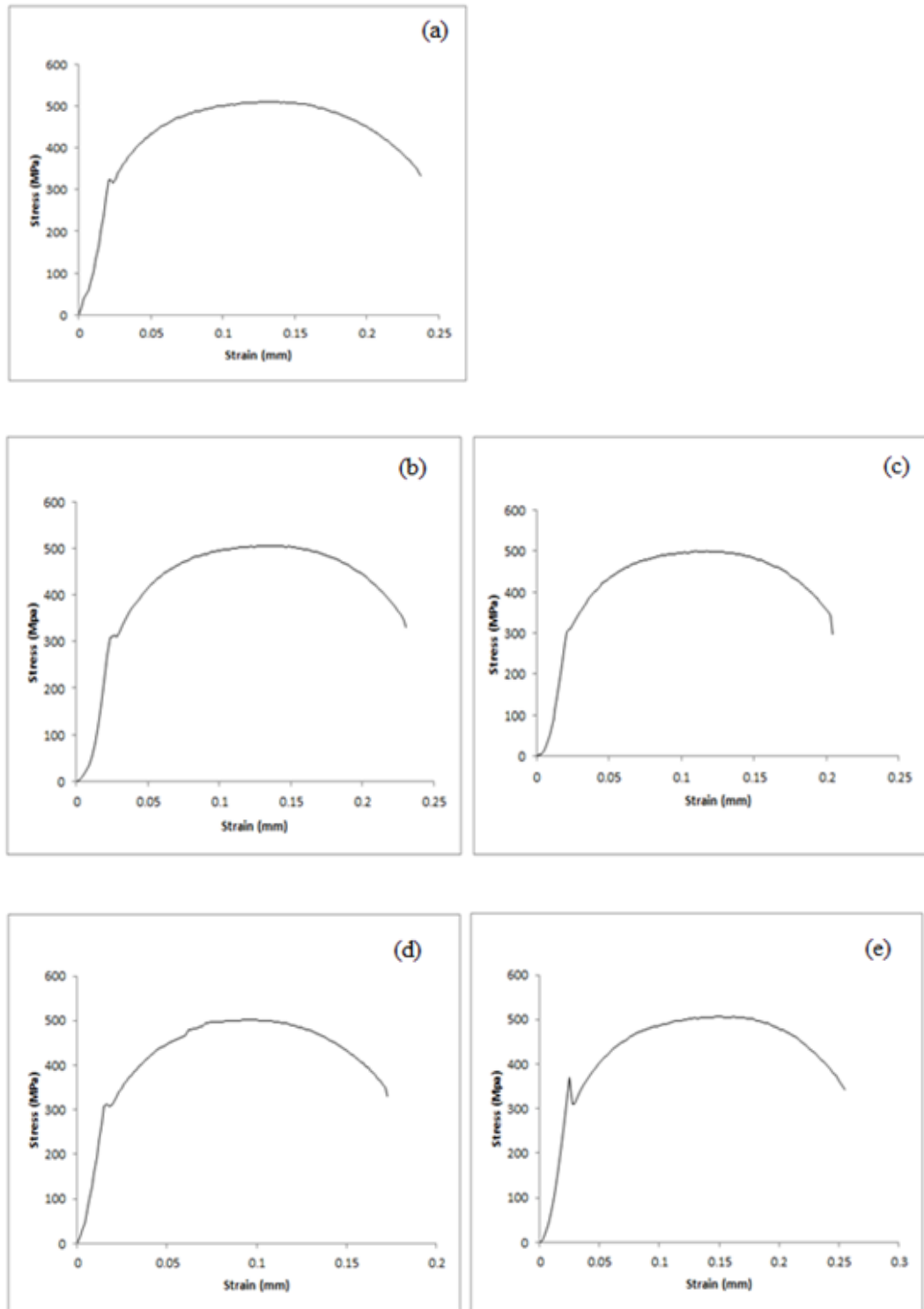


Figure 5.4: Stress-strain curves for the carbon steel specimens in different ethanol-water mixtures. (a) baseline, (b) no water, (c) 1 vol% water, (d) 2.5 vol% water and (e) 5 vol% water.

The stress-strain curves in Figure 5.4 show a discontinuous transition from elastic to plastic deformation. This heterogeneous yielding produces a distinct yield point, typical of low carbon steels. The curve for the specimen strained in ethanol with 5 vol% water (Figure 5.4 (e)) exhibited a well-defined yield point, indicating high ductility. This is in agreement with the percent elongation and area reduction in Table 5.1.

The curve for the carbon specimen in ethanol with 1 vol% water (Figure 5.4 (c)) shows an almost smooth transition from elastic to plastic deformation. A smooth stress-strain curve is primarily exhibited in less ductile materials. The curve in Figure 5.4 (c) would thus suggest that the carbon steel had low ductility in the test solution.

The ultimate tensile strength (UTS) of the base line was found to be about 509MPa. ASTM 516 Gr 60 typically has UTS that ranges between 415-550MPa. The observed value falls within this range. In the presence of ethanol-water solutions, the UTS reached for each test specimen was lower than 509MPa and varied as shown in Table 5.3. It is possible that the localised attack observed in Section 4.4 resulted in stress concentration and hence lowered the UTS.

Figure 5.4 (d) had the lowest area suggesting that carbon steel had low toughness in ethanol solutions with 2.5 vol% water. The calculated values of area were used to compare the toughness of the carbon specimens in the various ethanol-water solutions. The results are presented in Table 5.3 and Figure 5.5.

Table 5.3: UTS and energy absorbed before fracture.

Condition of experiment	UTS (MPa)	Energy absorbed (J)
Air	509.6	171.85
No water	505.6	122.64
1 vol% water	499.1	111.37
2.5 vol% water	502.6	59.19
5 vol% water	507.1	109.61

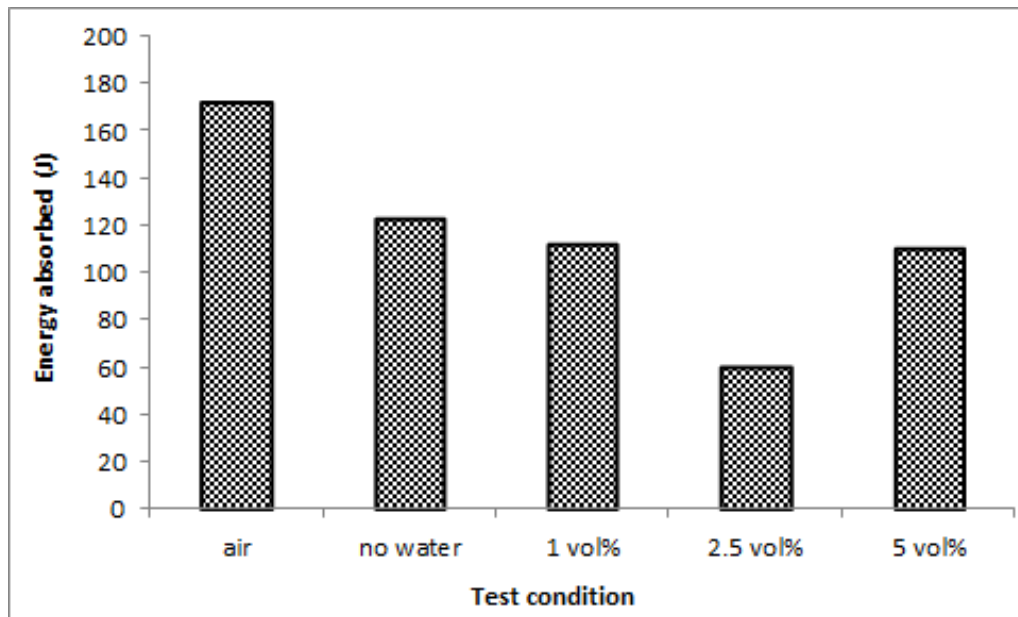


Figure 5.5: Energy absorbed under different experimental conditions.

There was a decrease in toughness with an increase in water content. The carbon steel in the solution with 5 vol% water exhibited higher toughness than the one in the ethanol with 2.5 vol% water. The graph in Figure 5.5 implies that carbon steel is most susceptible to SCC in ethanol solutions containing 2.5 vol% water.

5.4 Surface examination

The failed tensile specimens were examined under a stereo microscope. In all cases, the fractures were preceded by appreciable necking; typical of ductile fracture. The images of the failed samples are presented in Figure 5.6. The ductile nature of the fractures could imply that no SCC occurred since stress corrosion cracks exhibit characteristics of brittle fractures with little or no deformation.

Except for the tensile test piece exposed to the solution with 2.5 vol% water, none showed any surface cracks. The occurrence of SCC is associated with surface or subsurface tensile stresses (Robertson, 1956) and is therefore characterised by cracks that initiate at the surface as shown in Figures 2.4, 2.6 and 2.7. The cup-and-cone fracture observed on the test pieces implies that the fractures originated

from the centre near the axis of the applied stress, and propagated to the surface. In addition to this, the absence of surface cracks in the test piece exposed to the solution with 2.5 vol% water confirms that the cause of failure was simply ductile failure and not SCC.

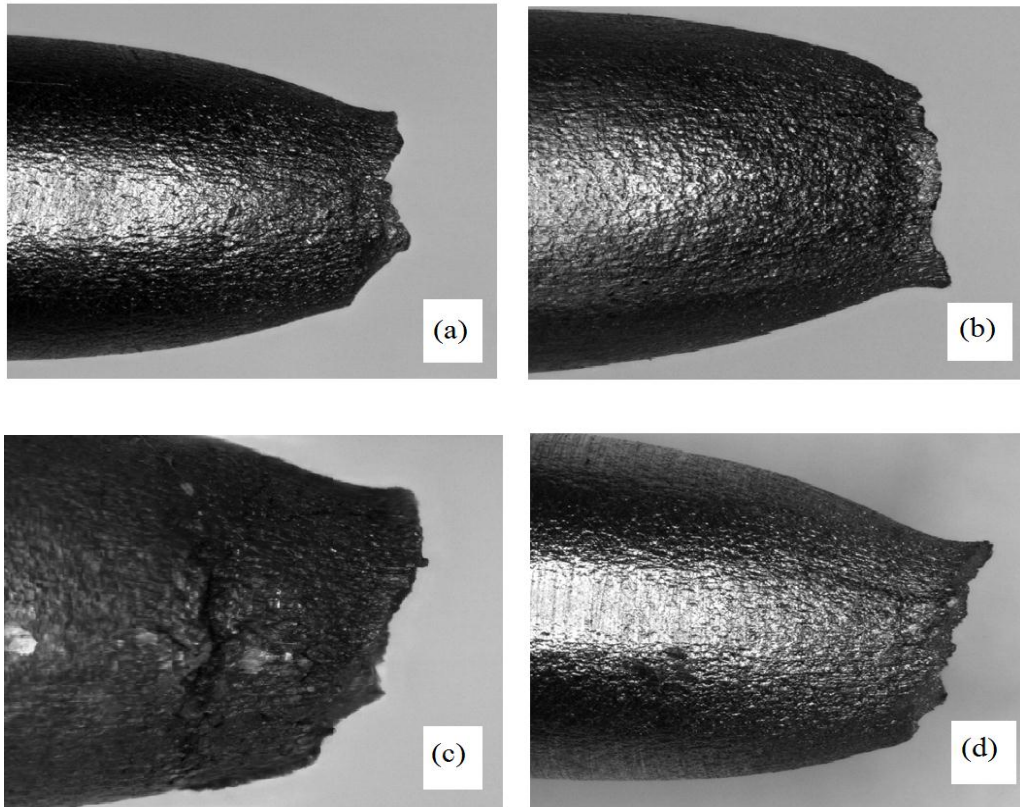


Figure 5.6: Fractured specimens. (a) No water, (b) 1 vol% water, (c) 2.5 vol% water and (d) 5 vol% water.

The crack on the sample exposed to the ethanol solution with 2.5 vol% water was mainly perpendicular to the direction of stress application and is multi-branched (Figure 5.6 (c)). This description is typical of cracks produced by SCC (Section 2.4.3). The cracked specimen was cut longitudinally and the cracked surface viewed under an optical microscope. The images seen are given in Figure 5.7.

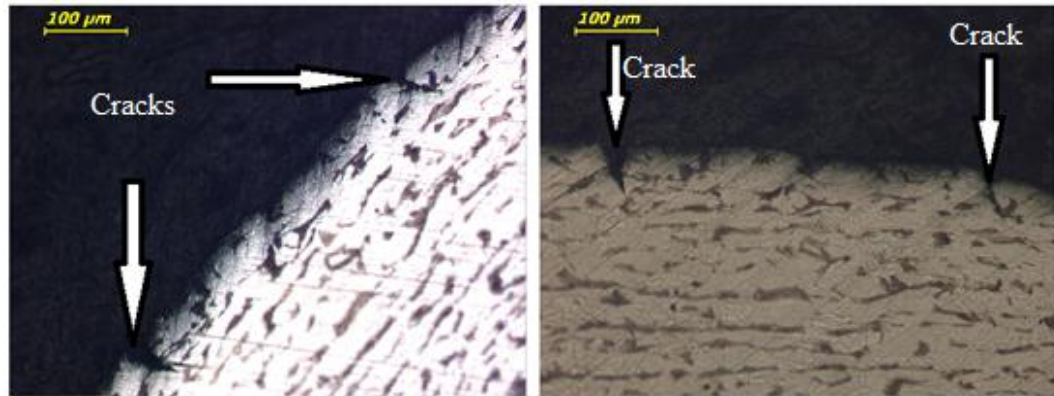


Figure 5.7: Surface cracks (indicated by arrows) on the carbon specimen viewed at different angles. 2% nital.

The cracks cut across the ferrite and pearlite grains, typical of TG-SCC (Figure 2.6). The average crack length was found to be 60.34 μm . Dividing the crack length by the time to failure gave a crack velocity of about 2.66×10^{-7} mm/s. This value is much greater than that observed by Lou (2010) (Figure 2.8).

SEM fractographs were obtained to study the crack on the test piece in the ethanol solution with 2.5 vol% water. The SEM fractographs are shown in Figure 5.8. The crack is multi-branched, as observed under the stereomicroscope.

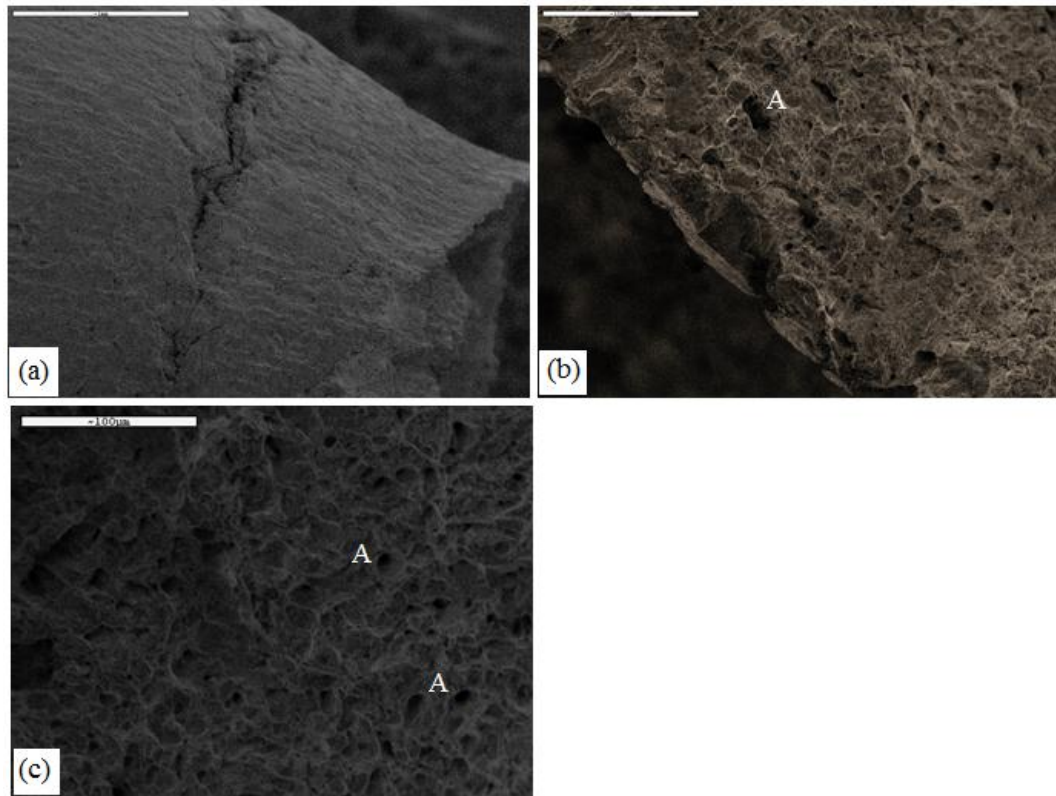


Figure 5.8: Fracture surface as viewed by SEM. (a) Crack morphology, (b) edge of fracture surface and (c) centre of fracture surface.

The centre of the fracture was characterised by shallow equiaxed dimples, indicating a ductile rupture under uniaxial tensile loading. Precipitates were observed in some of the dimples, marked by 'A' in Figures 5.8 (b) and (c). These particles probably acted as sites for microvoid nucleation. This is typical of ductile fracture (ASM, 1987). The reduction in area (Section 5.3) agrees with the appearance on the fracture surface. This is evidence that the failure of the specimen was due to ductile failure and not SCC.

CHAPTER SIX

CONCLUSIONS

The effects of water on the SCC of carbon steel in ethanolic media were studied by investigating how it influences the chemical properties of ethanol, the corrosion characteristics of carbon steel in ethanol-water mixtures and the tensile properties of carbon steel exposed to different ethanol-water mixtures.

The solution characterisation of ethanol-water revealed that adding water to ethanol increased oxygen content and the electrical conductivity but did not show any effect on the acidity of ethanol. The ethanol-water solutions exposed to carbon steel for short period of time did not show any measurable change in water content. However, exposure for longer period showed significant changes, indicating that the degradation of ethanol was time dependent.

The increase in conductivity and oxygen content was accompanied by an increase in the corrosiveness of ethanol as observed by the increase in corrosion rate in anhydrous ethanol with increase in water content. The corrosion mechanism of carbon steel was found to be charge transfer controlled in anhydrous ethanol, mixed in ethanol with 1 vol% and 5 vol% water and diffusion-controlled in solutions with 2.5 vol% water.

Despite the high oxygen quantities associated with ethanol solutions containing higher levels of water, corrosion in these solutions was seen to be characterised by low diffusion rates of oxygen to the corroding surface, leading to poor repassivation kinetics. The low diffusion rates implied mean that adding water to ethanol reduces the diffusion of oxygen in the solution, making it less prone to promote stable surface films. This was confirmed by the localised attack observed

on the corrosion specimens. The extent of attack was more severe in solutions with 1 and 5 vol% water.

The specimens subjected to SSRT were fairly ductile, exhibiting appreciable plastic deformation before fracture. The specimen in the ethanol solution with 2.5 vol% water displayed surface cracks perpendicular to the direction of stress application and satisfied the conditions of the NACE TM0111-2011 criterion for substantial SCC behaviour. However, the SEM fractographs revealed that the specimen in this solution had failed by ductile failure and not SCC. The specimens in solutions containing 0, 1 and 5 vol% water did not exhibit any SCC characteristics.

This work revealed that while the presence of water in ethanol enabled the initiation of various extents of corrosion, water contents of up to 5 vol% have no effect on the SCC susceptibility of carbon steel in ethanolic media.

Recommendations

Strain rate plays a significant role in the SCC of a metal in a given environment (Shier et al., 1994; Jarvis, 1994). It is recommended that further study be done using different strain rates to see if the conclusions drawn in this present work hold at any strain rate.

REFERENCES

Agarwal, A.K., 2007, 'Biofuels (alcohols and biodiesel) applications as fuels for internal combustion engines', *Progress in Energy and Combustion Science*, vol. 33, pp. 233-271.

Arup, H. & Parkins, R.N. (Ed.) 1975, *Stress corrosion research*, Nato Advanced Study Institute, Netherlands.

ASM, 1987, *ASM Handbook Vol. 12: Fractography*, 9th Edn., ASM International, Ohio, USA.

ASTM D6423 (2008), 'Standard test method for determination of phe of ethanol, denatured fuel ethanol, and fuel ethanol (Ed75-Ed85)', ASTM, West Conshohocken, USA.

ASTM G3-89 (2010), 'Standard practise for conventions applicable to electrochemical measurements corrosion testing', ASTM, West Conshohocken, USA.

ASTM G102 (1989) (Reapproved 1999), 'Standard practise for calculation of corrosion rates and related information from electrochemical measurements', ASTM, West Conshohocken, USA.

Beavers, J.A., Brogers, M.P., Agrawal, A.K. and Tallarida, F.A., 2008, 'Prevention of internal SCC in ethanol pipelines', Paper no. 08153, NACE Corrosion Conference & Expo 2008, accessed on 23 November 2011, http://www.dnvcolumbus.com/files/dsp_recent_publications_9_1_6.pdf

Bhola, S.M., Bhola, R., Jain, L., Mishra, B. and Olson, D.L., Corrosion behaviour of mild carbon steel in ethanolic solutions, *Journal of Materials Engineering and Performance*, vol. 20, no. 3, pp. 409-416.

Bio-Logic, 2011, Atlas of electrochemical nyquist diagrams: a guide to selected equivalent circuits, accessed 4 July 2012, www.bio-logic.info

Blue, G.D. and Moran, C.M., 1990, *Electrochemical corrosion studies in low conductivity media*, Astronautics Laboratory (AFSC), USA.

Brossia, C.S., 1995, 'The electrochemistry of iron in methanolic solutions and its relationship to corrosion', *Corrosion Science*, vol. 37, no. 9, pp. 1455-147.

Brown, B.F., 1977, *Stress Corrosion Cracking Control Measures*, Department of Commerce, National Bureau of Standards, Washington DC, USA.

Clubley, B.G. (Ed.), 1988, *Chemical inhibitors for corrosion control*, Royal Society of Chemistry, Manchester, UK, pp. 6, 73.

Codd, L.W., Dijkhoff, K., Fearon, J.H., Van Oss, C.J., Robernsen, H.C., and Stanford E.G. (Eds.), 1972, *Petroleum and Organic Chemicals*, Materials and Technology, vol. 4, Longman, USA, pp. 276-277.

Codd, L.W., Dijkhoff, K., Fearon, J.H., Van Oss, C.J., Robernsen, H.C., Stanford E.G. and Van Thoor, T.J.W. (Eds.), 1970, *Metals and Ores*, Materials and Technology, vol. 3, Longman, USA, pp. 791-795.

de Anna, P.L., 1985, The effects of water and chloride ions on the electrical behaviour of iron and 304L stainless steel in alcohols, *Corrosion science*, vol. 25, no. 1, pp. 43-53.

De Souza, J.P., Mattos, O.R., Sathler, L., Takenont, H., 1987, Impedance measurements of corroding mild steel in an automotive fuel ethanol with and without inhibitor in a two and three electrode cell, *Corrosion Science*, vol. 21, no. 21, pp. 1351-1364.

Ebrahim, N., Momeni, M., Kosari, A., Zakeri, M., and Moayed, M.H., 2012, 'Comparative study of critical pitting temperature (CPT) of stainless steels by electrochemical impedance spectroscopy (EIS), potentiodynamic and potentiostatic techniques', *Corrosion Science*, vol. 59, pp. 96-102.

Faraji, M., Farajtabar, A. and Gharib, F., 2009, 'Determination of water-ethanol mixtures autoprotolysis constants and solvent effects', *Journal of Applied Chemical Research*, vol. 9, pp. 7-12.

Fergusson, A., 2001, Ozone depletion and climate change: Understanding the linkages, Ministry of Public Works and Government Services, Canada, accessed on 26 December 2012, <http://expstudies.tor.gc.ca/e/ozone>

Fontana, M.G., 1986, Corrosion Engineering, 3rd Edn, McGraw-Hill, New York, USA.

Goodman, L. and Singh P.M., 2010, 'Effects of ethanol fuel on chemistry on SCC and passivation of pipeline steel', accessed on 23 November 2011, http://www.ipst.gatech.edu/students/posters/110309_goodman.pdf

Greene, N.D., 1965, *Electrode Kinetics*, Rensselaer Polytechnic Institute, New York, USA.

Herald, Sept 2012, SA introduces mandatory ethanol blending, New Ziana, accessed on 4 September 2012, www.zimpapers.co.zw

Hetényi, M. (Ed.), 1950, *Handbook of Experimental Stress Analysis*, John Wiley & Sons, New York, USA.

HILTI, 2000, Corrosion-Resistant Fastenings, accessed on 4 July 2012, <http://www.us.hilti.com/fstore/holus/LinkFiles/hilti.pdf>

Jarvis, A.R., 1994, Environmental assisted cracking (EAC) behaviour of a low alloy nickel in a sour environment, MSc Dissertation, University of the Witwatersrand, Johannesburg.

Kane, R.D., Maldonado, J.G. and Klein L.J., 2004, 'Stress corrosion cracking in fuel ethanol: A newly found phenomenon', Paper no.04543, Corrosion 2004, accessed on 23 November 2011, http://www.icorr.net/wpcontent/uploads/2011/01/Ethanol_SCC.pdf

Karpenko, G.V. and Vasilenko, I.I., 1979, *Stress Corrosion Cracking of Steels*, Transtech Publication, Switzerland.

Khuri, A.I., 2003, *Advanced Calculus with Application in Statistics*, 2nd Edn., John Wiley & Sons, New Jersey, USA.

Knott J.F. and Withey P.A., 1993, *Fracture Mechanics: Worked Examples*, 2nd Edn., The Institute of Materials, London, UK.

Lapede, D.N., 1978, Dictionary of scientific and technical terms, 2nd Edn., McGraw Hill, New York, USA, pp. 918.

Lou, X., 2010, Stress corrosion cracking and corrosion of carbon steel in stimulated fuel-grade ethanol, PhD dissertation, Georgia Institute of Technology, accessed on 23 November, 2011, <http://gateway.proquest.com>

Lou, X. and Singh, P.M., 2011, 'Corrosion and pitting behaviour of carbon steel in simulated fuel-grade ethanol under variations in ethanol chemistry', accessed on 3 December 2011, <http://www.onepetro.org/mslib/servlet/onepetropreview>

Lou, X., Yang, D. and Singh, P.M., 2009, 'Effects of ethanol chemistry on stress corrosion cracking of carbon steel in fuel-grade ethanol', *Corrosion*, vol. 65, no.12, pp. 785-796.

Macdonald, J.R., 1992, 'Impedance spectroscopy', *Annals of Biomedical Engineering*, vol 20, pp. 289-305.

McMurry, J., 2007, *Organic Chemistry: A Biological Approach*, Thomson Books, Belmont, California, USA.

Metrohm, 2011, Autolab Application Notes, accessed on 4 July 2012 <http://www.ecochemie.nl/export/Homepages/Autolab/download/Applicationnotes>

Metzge, R.M., 2012, *The Physical Chemist's Toolbox*, John Wiley & Sons, New Jersey, USA.

NACE Standard TM0111-2011, '*Standard test method: slow strain rate test method for evaluation of ethanol stress corrosion cracking in carbon steels*', NACE International, Houston, USA.

Naik, S.N., Vaibhav, V.G., Prasant, K.R. and Ajay, K.D., 2010, Production of first and second generation biofuels: A comprehensive review, renewable and sustainable energy reviews, vol. 14, pp. 578-597, accessed on 10 November 2012, <http://efwscientists.com/WordPress/wp-content/>

NPL, 2000, Guidelines to good practice in corrosion control: Stress corrosion cracking, accessed on 17 November 2011, <http://www.npl.co.uk>

Newman, R.C., 2008, 'Review and hypothesis for the stress corrosion mechanism of carbon steels in alcohols', *Corrosion*, vol. 64, no.11, p 819-824.

Nygaard, P.V., 2008, Non-destructive electrochemical monitoring of reinforcement corrosion, PhD Thesis, Technical University of Denmark, accessed on 8 July 2012, <http://www.byg.dtu.dk/upload/institutter/byg/publications/rapporter/byg-r202.pdf>

Obuka, N.S., Okoli, N.C., Ikwu G.R. and Chukwumuanya, E.O., 2012, 'Review of corrosion kinetics and thermodynamics of CO₂ and H₂S corrosion effects and associated prediction/evaluation on oil and gas pipeline steel', *International Journal of Scientific and Technology Research*, vol. 1, no. 4, p. 156-162.

ORNL, 2008, 'Ethanol pipeline corrosion literature study: Final report', accessed on 23 November 2011, <http://www.ornl.gov/sci/ees/itp/documents/ORNL>

Osterman, K., 2012, 'Stainless steels: cost effective materials', *Ethanol Producer Magazine*, accessed on 26 December 2012, <http://ethanolproducer.com/articles/8853/stainless-steels-cost-effective-materials>

Perry, R.H. and Green D.W. (Ed.), 1999, *Perry's Chemical Engineers' Handbook*, 7th edn, McGraw-Hill, USA.

Pletcher, D., 1991, *A First Course in Electrode Processes*, The Electrochemical Consultancy, England.

REM, 2012, Global ethanol production to top 85billion litres in 2012, Renewable Energy Magazine, accessed on 29 December 2012, www.renewableenergymagazine.com/article/global-ethanol-to-top-85-billion

Reseder, R.S.T. (Ed.), 1980, *NACE Corrosion Engineer's Reference Book*, NACE International, Houston, USA.

Revie, R.W. (Ed.), 2011, *Uhlig's Corrosion Handbook*, John Wiley and Sons, New Jersey, USA.

RFA, 2012, Accelerating Industry Innovation: 2012 Ethanol Industry Outlook, accessed on 10 November 2012, <http://ethanolrfa.3cdn.net>

Rhodin, T.N. (Ed.), 1959, *Physical Metallurgy of Stress Corrosion Fracture*, Metallurgical Society Conferences, AIME, Pennsylvania, USA.

Roberge, P.R., 2008, *Corrosion Kinetics and Application of Electrochemistry to Corrosion*, McGraw Hill, New York, USA.

Robertson, W.D., 1956, *Stress Corrosion Cracking and Embrittlement*, John Wiley, New York, USA.

Roelf, W., 2012, 'South Africa sees \$ 258mln ethanol plant by 2014', Reuters US Edition accessed on 3 March 2012, <http://news.yahoo.com/africa-sees-258-mln-ethanol-plant-2014-112718876.html>

Rosenblim, L., Scheuermann, C., Barrett, C.A. and Lowdermilk, W.H., 1968, 'Mechanism and kinetics of corrosion of selected iron and cobalt alloys in refluxing mercury', NASA, Washington DC, accessed on 26 December, 2012 <http://www.researchgate.net/publication/24334555>

Scheel, J., September 2010, 'Eliminating stress corrosion cracking in stainless steels', *Metal Finishing News*, vol. 11, accessed on 3 March 2012, <http://mfn.li/article/?id=898>

Schweitzer, P.A., 2010, *Fundamentals of Corrosion: Mechanism, Causes and Preventative Methods*, CRC Press, New York, USA.

Scribner, L.A., 2001, 'Corrosion by organic acids', *Corrosion*, accessed on 17 January 2012, www.onepetro.org/mslib/servlet/onepetropreview

Shier, L.L., Jarman, R.A. and Burstein, G.T., 1994, *Corrosion Volume 1: Metals/Environment Reactions*, 3rd edn, Butterworth Heinemann, Oxford.

Sherratt, M.S., 1992, Corrosion monitoring using electrochemical noise, LPR, ZRA and AC impedance techniques, MSc Dissertation, University of the Witwatersrand, Johannesburg, RSA.

Simbi, D.J., 2006, Lecture notes distributed in Corrosion engineering MG415, University of Zimbabwe, Harare, Zimbabwe, on February 2006.

Song, H. and Saraswathy, V., 2007, 'Corrosion monitoring of the reinforced concrete structures: A review', *International Journal of Electrochemical Science*, vol. 2, pp. 1-20.

Spitzer, P., Fisicaro, P., Seitz, S. and Champion, R., 2009, 'pH and the electrolytic conductivity as parameters to characterize bioethanol', *Accred. Qual. Assur.*, vol. 14, pp. 617-676, accessed on 3 March 2012, <http://link.springer.com/content/pdf>

Sridhar, N., Price, K., Buckingham, J. and Dante, J., 2006, 'Stress corrosion cracking of carbon steel in ethanol', *Corrosion*, vol. 62, no. 8, pp. 687-702.

Stassa, 2012, Census 2011 Statistical Release P0301.4, Statistics South Africa, Pretoria, accessed on 26 December 2012, www.statssa.gov.za

Tembe, S.M., 2010, Low temperature oxidation of ethanol to acetic acid using gold based catalysts, MSc Dissertation, University of Witwatersrand, Johannesburg, RSA.

Thompson, N.G. and Lawson, K.M., 1991, An electrochemical method for detecting ongoing corrosion of steel in a concrete structure with cathodic protection applied, Strategic Highway Research Program, National Research Council, Washington DC, USA.

Thompson, N.G., Lawson, K.M. and Beavers, J.A., 1988, 'Monitoring cathodically protected steel in concrete structures with electrochemical impedance techniques', *Corrosion Engineering*, vol. 44, no. 8, pp. 581-588.

Uhlig, H. (Ed.), 1948, *Corrosion Handbook*, John Wiley & Sons, London.

UN-Energy, 2011, Ethanol Fuel in Brazil, *Energy Stories*, accessed on 2 January 2013, <http://www.un-energy.org/stories/38-ethanol-fuel-in-brazil>

Van der Merwe, J.W., 2011, Introduction to corrosion, Lecture notes distributed in Weldability of steels and stainless steels CHMT7050, University of Witwatersrand, Johannesburg on 12 September 2011.

Yahalom, J. and Aladjem, A., 1980, Stress Corrosion Cracking, Freund Publishing House, Israel.

Yates, P., 2005, Chemical Calculations at a Glance, Blackwell Publishing, England.

Young, W.C., 1989, Roark's formulas for stress and strain, 6th Edn., McGraw Hill, UK.

APPENDICES

Appendix A

Water content estimation

Apparatus:

oven, funnel, filter paper, crucible, timer, measuring scale.

Procedure:

1. Dry crucible in oven at approximately 100°C for at least 5 minutes.
 2. Allow the crucible to cool and then measure its mass (m_1).
 3. Add sodium chloride and weigh (m_2).
 4. Place the crucible in the oven and dry the salt for about 20 minutes.
 5. Allow to cool and weigh (m_3). If $m_3 - m_2$ is less than 0.003 g, proceed. Otherwise, place in the oven and dry further.
 6. Dissolve the salt in 50 mL of the solution whose composition is to be determined.
 7. Shake thoroughly for ± 4 minutes.
 8. Filter. Place residue in the oven for 45-60 minutes.
 9. Weigh a dry crucible (m_4).
 10. Place dried residue in the dry crucible, allow to cool and weigh (m_5)
- The mass of the salt that has dissolved is given by $[(m_3 - m_1) - (m_5 - m_4)]$. The solubility of sodium chloride is thus expressed as this mass per 50 mL.

Statistical analysis

The t-distribution was used to generate a confidence interval. A total of 15 repeats were measured for solutions with 60 v% water and the solubility of each was

determined. The water contents corresponding to these solubility values were estimated from the calibration curve in Figure A.1 and used to generate Table A.1.

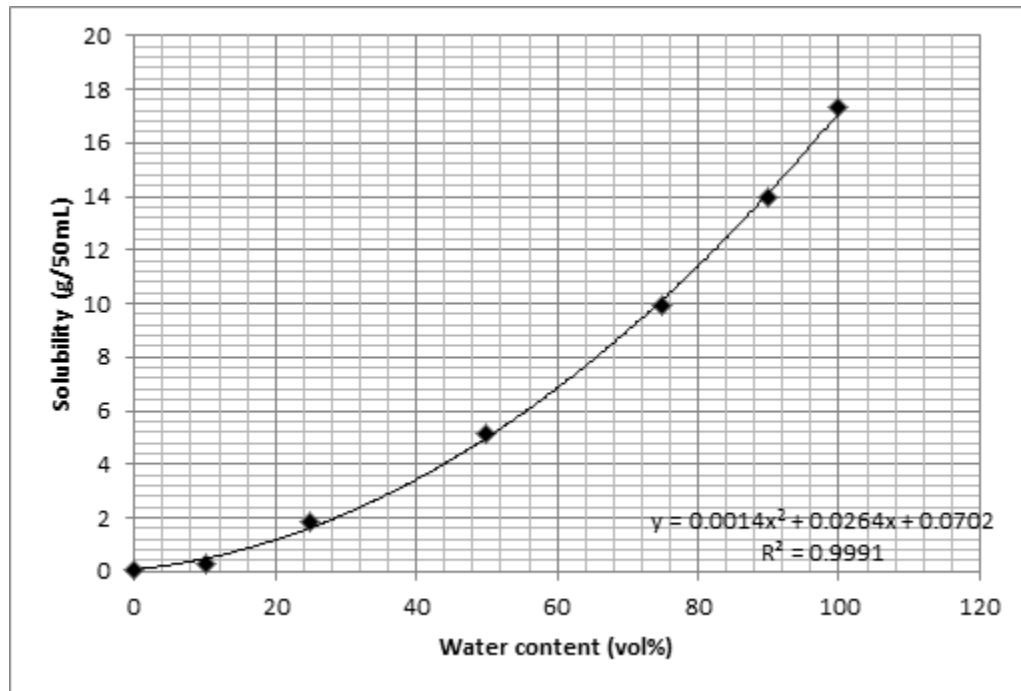


Figure A.1: Calibration curve relating solubility and water content.

$$\begin{aligned} \text{Variance, } s^2 &= \frac{\sum(x_i - x_{\text{mean}})^2}{n-1} \dots\dots\dots \text{A.1.} \\ &= 0.8675 \end{aligned}$$

The standard deviation, s , is therefore $= \sqrt{0.8675}$
 $= 0.9314$

The confidence level is given by Equation A.2.

$$\text{Confidence interval} = \frac{t \times s}{\sqrt{n}} \dots\dots\dots \text{A.2.}$$

Using two standard deviations as a reasonable estimate of uncertainty, the confidence level is taken as 95%. For 14 degrees of freedom, $t = 2.14$ (Yates, 2005)

$$\text{Therefore, confidence interval} = \frac{2.14 \times 0.9314}{\sqrt{14}}$$

$$= 0.53269$$

Then the estimated value of water content = $57.08 \pm 0.53\text{v}\%$

This confidence was applied to all estimated values.

Table A.1: Statistical analysis of water content estimates.

Sample number	Estimated water content (v%), x_i	$x_i - x_{mean}$	$(x_i - x_{mean})^2$
1	58.564	1.487	2.212
2	55.137	-1.940	3.762
3	57.153	0.0755	0.0057
4	58.307	1.229	1.512
5	56.889	-0.188	0.0353
6	56.598	-0.479	0.230
7	57.034	-0.043	0.0018
8	56.430	-0.647	0.419
9	56.462	-0.615	0.378
10	57.894	0.817	0.667
11	56.896	-0.182	0.0333
12	57.564	0.487	0.237
13	57.798	0.721	0.520
14	57.681	0.604	0.365
15	55.748	-1.329	1.765
x_{mean}	57.077		

Appendix B

SSRT

Calibration of the SSRT motor

To calibrate the motor, the strain rate was determined at different frequencies by Equation B.1.

$$\text{Strain rate} = \frac{\text{strain}}{\text{time in seconds}} \dots\dots\dots \text{B.1}$$

and strain is given by

$$\text{Strain} = \frac{\text{final specimen length} - \text{original length}}{\text{original length}} \dots\dots\dots \text{B.2}$$

The obtained results are shown in Table B.1 and were used to plot a calibration curve shown in Figure B.1.

Table B.1: Calibration of the stepper motor.

Frequency (Hz)	Strain	Time (s)	Strain rate $\times 10^{-6}$ (s^{-1})
20	0.06290	182220	0.345187
40	0.10714	106200	1.00888
60	0.18723	137500	1.36167
80	0.20146	92460	2.17889
100	0.23850	76800	3.10547

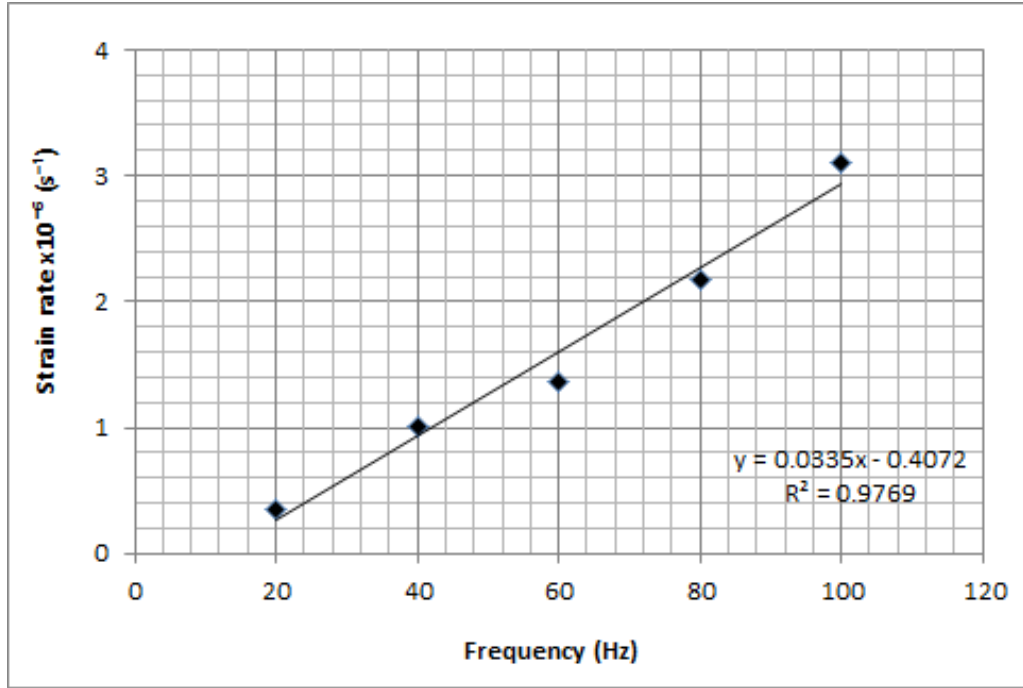


Figure B.1: Calibration curve relating frequency and strain rate.

Stress-strain curves

The SSRT data was collected as load against time. To convert load to stress, Equation B.3 was used.

$$\text{Stress (MPa)} = \frac{\text{Force}}{\text{Cross sectionnal area of specimen}} \quad \text{.....B.3}$$

$$\text{where Force (N)} = \text{Load in kg} \times 9.81 \text{ N kg}^{-1} \quad \text{.....B.4}$$

$$\text{and Area (mm}^2\text{)} = \pi \frac{D_0^2}{4} \quad \text{.....B.5}$$

The stresses obtained by these equations were based on the original diameter of the specimen D_0 .

Instantaneous strain at time, t , was calculated by Equation B.6.

$$\text{Instantaneous strain} = \varepsilon \times t \quad \text{.....B.6}$$

This instantaneous strain is an estimation of the actual values but for the purpose of comparison, it sufficed. The values of stress (by Equation B.3) and those of strain (by Equation B.6) were used to plot the stress-strain curves in Figure 5.4.

Energy calculations

The energy absorbed before fracture was estimated by calculating the area under the stress-strain curves in Figure 5.4. The Trapezoidal method was used for this purpose. Consider Figure B.2 which shows one of the stress-strain curves.

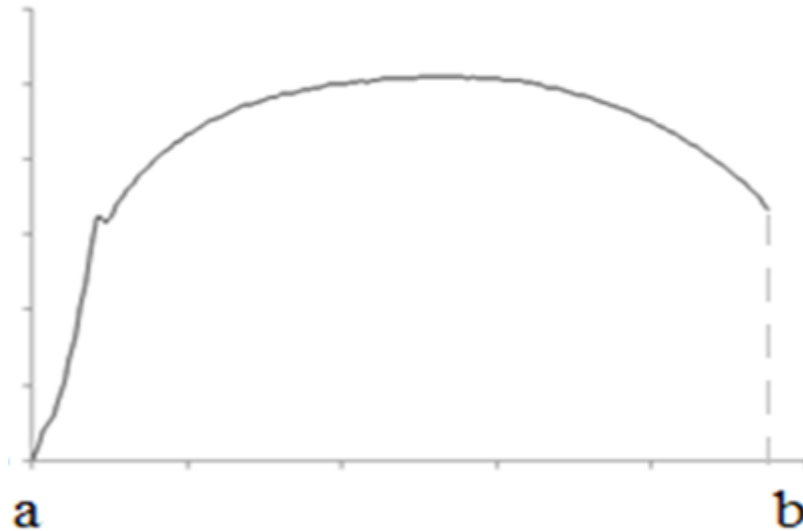


Figure B.2: A typical stress-strain curve.

The area under the curve can be represented as an integral of the form $\int_a^b f(x)dx$. The interval from **a** to **b** (Figure B.2) was divided into n equal parts by the partition points $a = x_0, x_1, x_2, \dots, x_n = b$. The area of the i th trapezoid lying between x_{i-1} and x_i is given by

$$A_i = \frac{h}{2} [f(x_{i-1}) + f(x_i)] \quad i = 1, 2, \dots, n \quad \dots\dots\dots \text{B.7}$$

Where h is the width of the trapezium.

The approximation of the integral $\int_a^b f(x)dx$ is given by Equation B.8

$$A = \frac{h}{2} [f(x_0) + f(x_n) + 2 \sum_{i=1}^{n-1} f(x_i)] \quad \dots\dots\dots \text{B.8}$$

(Khuri, 2003)

Ductility

Ductility was expressed as percent elongation and area reduction calculated according to Equations B.9 and B.10.

$$\% \text{ elongation} = \frac{\text{Final length of specimen} - \text{original length}}{\text{original length}} \dots\dots\dots \text{B.9}$$

$$\% \text{ area reduction} = \frac{\text{Original area of specimen} - \text{final area}}{\text{original area}} \dots\dots\dots \text{B.10}$$